DELAYED BIFURCATION ONSET OF TURING INSTABILITY AND THE EFFECT OF NOISE

by

Chunyi Gai

Submitted in partial fulfillment of the
requirements for the degree of
Master of Science

at

Dalhousie University
Halifax, Nova Scotia
December 2015

Table of Contents

List of Figures

Abstract

In this thesis we study the effect of noise on delayed bifurcations in PDE's. Two particular problems with slowly varying parameter and noise are considered: a single PDE and a modified version of Klausmeier model. We first study the combined effect of spatio-temporal noise and slowly varying parameter on the onset of the Turing bifurcation. The noise helps to trigger the spatially inhomogeneous instability, and we compute the delay in this instability. We review and extend the results of [1], to more general situations, and also analyse the full distribution of the blowup time. We also analyse the case where spatio-temporal noise is replaced by purely spatial noise and we obtain the asymptotic density distribution of blow up time in the case where the domain is sufficiently small. Full numerical simulations are used to validate our analytical results.

Acknowledgements

I would first like to thank my supervisor, Theodore Kolokolnikov, for accepting me as a student and introducing me to this interesting project. I really appreciate the patience, encouragement and professional guidance he provided to me. As a student with little experience in writing papers, he also provided me with many corrections. Without his instructions, this thesis could not have reached its present form. I would also like to thank my senior fellow student Shuangquan Xie, for discussing the questions and making suggestions during the project. Many thanks as well to my fellow students for help and support when needed.

Chapter 1

Introduction

In stability and bifurcation analysis, the bifurcation parameter is usually assumed to be independent of time. However, in many experiments, the bifurcation parameter is not constant but rather slowly changing, and there are many examples of this in physics [2, 3], engineering, biology [4] and ecology [5, 6, 7]. One of the most important and interesting phenomena of this class of dynamical systems is that the slow parameter drift can cause a delay in bifurcation: the trajectory of the full system does not jump at the exact bifurcation point but is delayed as if it has memory of former states. Delayed bifurcation was first introduced in [8, 9], and there is a growing body of literature on the analysis of this phenomenon, especially in the context of ODE's (see [10] for a recent overview of the subject and references therein). In the context of PDE systems, J. C. Tzou et al. studied delayed bifurcations for spike solutions of three reaction-diffusion systems [11].

Recent studies have shown that noise also has an important effect on the transition from homogeneous states to patterns through instability. The influence of noise on a delayed bifurcation was theoretically investigated in [12, 13], where the Langevin equation was analyzed by the method of moments, and in [14, 15], where the Fokker-Plank equation was obtained and the probability density function was used to find the delayed bifurcation points. In general, delay in bifurcation can be reduced by noise even to the extent that the bifurcation point can occur before the static bifurcation point [16].

There is a growing body of literature on the effect of noise on delayed bifurcation with different applications such as climate change [17, 18, 19] and laser dynamics [20, 21]. Most of this work was done on ODE's. More recently, in [1], we considered a slow passage problem through a Turing bifurcation, where a modified reaction-advection-diffusion system from Klausmeier model for vegetation patterns with Gaussian white noise was studied.

The goal of this thesis is to review and to give some extensions of the results in [1], which concerns delayed bifurcation for a system of PDE's in the presence of noise. We study two PDE models with slowly varying parameters and additive Gaussian white noise. The first model is a warm-up problem which consists of a single equation of the following form:

$$\begin{cases} u_t = u_{xx} + a(\varepsilon t)u - u^3 + noise, \quad x \in (0,\pi), \\ u(0,t) = u(\pi,t) = 0. \end{cases} \tag{1.1}$$

The noise in (1.1) is Gaussian white noise and is modeled as

$$noise = \sigma_0 \frac{dW}{dt}, \tag{1.2}$$

where σ_0 is the intensity of noise and dW is spatio-temporal Wiener process defined by [22]

$$dW = \sqrt{dt} \sum_{m=0}^{\infty} \xi_m(t) \exp(imx),$$

of which $\xi_m(t)$ is a normal distributed random variable (with mean zero and variance one).

The corresponding ODE model is $u_t = au - u^3$, and it undergoes a supercritical pitchfork bifurcation as a is increased past the pitchfork bifurcation point [23], and the effect of noise on the delayed bifurcation is studied by R. Kuske [15], S. Varela, et al. [16], and Nils Berglund, Barbara Gentz [24].

The second model is a modified Klausmeier model that was studied in [1]. It was first introduced by Klausmeier in [25], and models the dynamics between plant and water in semiarid regions on ecologically realistic assumptions. Many subsequent models incorporate more specific details of this process. For example in [26, 27], one of the variables which denotes water is separated as two variables–soil water and surface water; some authors have also included rainfall variability [28, 29]. See [30] and references therein for a recent overview of Klausmeier model. In this thesis, we use a modified version of vegetation pattern formation system which has the following non-dimensional form:

$$\begin{cases} \frac{\partial n}{\partial t} = \delta \frac{\partial^2 n}{\partial x^2} + n^2 w - n, \\ b\frac{\partial w}{\partial t} = d\frac{\partial^2 w}{\partial x^2} + c\frac{\partial w}{\partial x} + a(\varepsilon t) - w - n^2 w + noise, \end{cases} \tag{1.3}$$

where $n(x,t)$ denotes plant density and $w(x,t)$ corresponds to soil water concentration. In the model, $\delta\frac{\partial^2 n}{\partial x^2}$ denotes spread of plants and $d\frac{\partial^2 w}{\partial x^2}$ denotes the diffusion of water within soil; $c\frac{\partial w}{\partial x}$ denotes downhill water flow. The parameter b represents the differing timescales in changes in water level (in days, say) versus those in plant density (in months). Parameter a represents the precipitation, and we consider what happens as it is slowly decreased in time, thus we model it as

$$a = a_0 - \varepsilon t, \quad 0 < \varepsilon \ll 1. \tag{1.4}$$

The initial precipitation a_0 is assumed to be sufficiently large so that the system has full vegetation cover (corresponding to the nontrivial spatially homogeneous state) when $a(0) = a_0$. Moreover, there exists a Turing bifurcation point $a = a_p < a_0$ (where a_p is derived in §2.1, see equation (2.11) there). Eventually, as a is decreased below a_p, this bifurcation is triggered. However it is fully manifested for values of a well below a_p. The delay in this bifurcation is the subject of this thesis.

1.1 Thesis outline and main contributions

The outline of this thesis is as follows. In §2, we give a brief review of the main tools used in this thesis. This includes Turing instability, delayed bifuractions, and a derivation of Fokker Planck PDE. In §3 we consider two slow passage problems with Gaussian white spatio-temporal noise. In §3.1, we study the warm-up problem (1.1) and characterize the distribution of blow up time. In §3.2, we consider the Klausmeier model (1.3) in one dimension. We first discuss the system with noise under the assumption that $b = 0$, $c = 0$. We summarize the methods used in [1] to obtain an analytical threshold at which the variance of this density starts to grow exponentially by using the Fokker-Planck PDE and solving for the density distribution function. We also compare the full numerics and asymptotic results for different precipitation rate ε. In §3.3 and §3.4, more general cases ($b \neq 0$ and $c \neq 0$) are considered and new blow up time is obtained. We also verify these results using full numerics. The results of §3 are based on [1].

In §4, we consider the case where the spatio-temporal noise is replaced by a purely spatial noise. We first consider a linear deterministic ODE including a slowly changing bifurcation parameter and random variable. We then obtain a *canonical* distribution

of blow-up time (see Theorem 1). In §4.2 and §4.3, we apply Theorem 1 to the two PDE problems studied in §3 with spatial noise by reducing them to the same form as the linear deterministic ODE, and conclusions about density distributions of blow up time are obtained with some scaling. Additionally, we compare the density function obtained by analysis and the full numerical results. Ultimately, we conclude by discussing our results and some future work in §5.

There have been many related works dealing with the effect of noise to delayed bifurcation for ODE's. On the other hand, much less is known about it in the context of PDE's [1]. The main difference between these past results and this current thesis is that we obtain the distribution of the delay in bifurcation of the single PDE rather than ODE. Also, we generalise the results of [1] to the more general reaction diffusion systems. In addition, the noise is usually regarded as spatio-temporal noise, and very little is known about dynamical systems for PDE systems driven by purely spatial Gaussian white noise. In §4, we conduct the analysis of noisy delayed bifurcations for PDE's with delay in the bifurcation with purely spatial noise to obtain the distribution of the blow up time in some simple cases.

Chapter 2

Brief reviews of Turing analysis and Fokker Planck PDE

2.1 Pattern formation and Turing instability

In this section we review Turing's analysis of the stability of spatially uniform steady-state solutions, which is named after Alan Turing, who in 1952 showed that an initially stable steady-state of a dynamical system can become unstable if diffusion is added to the system, and patterns are formed through the instability of the homogeneous steady-state to small spatial perturbations [31]. It is a surprising and unexpected phenomenon because diffusion usually has a smoothing effect. The loss of stability due to diffusion is called Turing instability.

We first consider a single one-dimensional PDE with Neumann boundary condition.

$$\begin{cases} u_t = Du_{xx} + f(u), \quad x \in (0, L) \\ u'(0) = u'(L) = 0. \end{cases} \tag{2.1}$$

Suppose $\bar{u}$ is a stable steady state of the ODE $u_t = f(u)$, so that $f(\bar{u}) = 0$ and $f'(\bar{u}) < 0$. Now add small perturbations around $\bar{u}$, i.e., $u = \bar{u} + e^{\lambda t}\phi(x)$, where $|\phi| \ll 1$. If small perturbations from the steady-state converge back to the steady-state, i.e., $\lambda < 0$, then we say that the homogeneous steady-state solution is stable. Plugging $u = \bar{u} + e^{\lambda t}\phi(x)$ into (2.1) we obtain

$$\begin{cases} \lambda\phi = D\phi_{xx} + f'(\bar{u})\phi, \\ \phi'(0) = \phi'(L) = 0. \end{cases} \tag{2.2}$$

Solving for ϕ in (2.2) yields $\phi = \cos(mx)$, where $m = \frac{k\pi}{L}$ and $k = 0, 1, 2, \ldots$, and $\lambda = -m^2 D + f'(\bar{u}) < 0$. Thus $\bar{u}$ is still stable with the diffusion term.

Now we consider the following reaction diffusion system:

$$\begin{cases} u_t = D_1 u_{xx} + f(u, v), \quad x \in (0, L) \\ v_t = D_2 v_{xx} + g(u, v), \quad x \in (0, L) \\ u'(0) = u'(L) = v'(0) = v'(L) = 0; \end{cases} \tag{2.3}$$

where D_1, D_2 are positive constants. Suppose (2.3) has a homogenous steady state $(\bar{u}, \bar{v})$ which satisfies

$$f(\bar{u}, \bar{v}) = 0, \quad g(\bar{u}, \bar{v}) = 0.$$

Moreover, we suppose $(\bar{u}, \bar{v})$ are stable for the corresponding ODE system

$$\begin{cases} u_t = f(u, v), \\ v_t = g(u, v). \end{cases} \tag{2.4}$$

Now we linearize u, v in (2.4) as $u = \bar{u} + e^{\lambda t}\phi$ and $v = \bar{v} + e^{\lambda t}\psi$, and plug the expressions in (2.4) to obtain

$$\lambda \begin{pmatrix} \phi \\ \psi \end{pmatrix} = J \begin{pmatrix} \phi \\ \psi \end{pmatrix},$$

where $J = \begin{pmatrix} f_u(\bar{u}, \bar{v}) & f_v(\bar{u}, \bar{v}) \\ g_u(\bar{u}, \bar{v}) & g_v(\bar{u}, \bar{v}) \end{pmatrix}$ is the Jacobin matrix. The eigenvalues satisfy

$$\lambda^2 - \text{trace}(J)\lambda + \det(J) = 0.$$

Since $(\bar{u}, \bar{v})$ is assumed to be stable, we have $\text{trace}(J) < 0$ and $\det(J) > 0$, i.e., $f_u + g_v < 0$ and $f_u g_v - g_u f_v > 0$.

Next we linearize u, v in (2.3) as $u = \bar{u} + \sum_{m=0}^{\infty} \cos(mx) e^{\lambda t}\hat{\phi}$ and $v = \bar{v} + \sum_{m=0}^{\infty} \cos(mx) e^{\lambda t}\hat{\psi}$, where $\hat{\phi}, \hat{\psi}$ are constants and $|\hat{\phi}|, |\hat{\psi}| \ll 1$, $m = \frac{k\pi}{L}$, $k = 0, 1, 2, \ldots$. Plugging all the expressions into (2.3) and we obtain

$$\lambda \begin{pmatrix} \hat{\phi} \\ \hat{\psi} \end{pmatrix} = \begin{pmatrix} -D_1 m^2 + f_u(\bar{u}, \bar{v}) & f_v(\bar{u}, \bar{v}) \\ g_u(\bar{u}, \bar{v}) & -D_2 m^2 + g_v(\bar{u}, \bar{v}) \end{pmatrix} \begin{pmatrix} \hat{\phi} \\ \hat{\psi} \end{pmatrix},$$

denote $M = \begin{pmatrix} -D_1 m^2 + f_u(\bar{u}, \bar{v}) & f_v(\bar{u}, \bar{v}) \\ g_u(\bar{u}, \bar{v}) & -D_2 m^2 + g_v(\bar{u}, \bar{v}) \end{pmatrix}$, then λ satisfies

$$\lambda^2 - \text{trace}(M)\lambda + \det(M) = 0.$$

Similarly we have $(\bar{u}, \bar{v})$ is stable in (2.3) when $\text{trace}(M) < 0$ and $\det(M) > 0$. Since $(\bar{u}, \bar{v})$ is stable in the corresponding ODE system, we have $\text{trace}(M) = f_u + g_v - (D_1 + D_2)m^2 < 0$ is always true, thus $(\bar{u}, \bar{v})$ is stable in (2.3) if $\det(M) > 0$ for

all $m > 0$ and unstable if $\det(M) < 0$ for some $m > 0$, where $\det(M)$ is a quadratic function which can be written as

$$\det(M) = Q(m^2) = D_1 D_2 m^4 - (D_1 g_v + D_2 f_u) m^2 + f_u g_v - f_v g_u.$$

More specifically, the instability exists if and only if $D_1 g_v + D_2 f_u \geq 0$ and $(D_1 g_v + D_2 f_u)^2 - 4 D_1 D_2 (f_u g_v - f_v g_u) > 0$.

To illustrate Turing instability more clearly, we perform Turing analysis on the Klausmeier model (1.3) with the assumption that $b = 0, c = 0, d = 1$ and constant a:

$$\begin{cases} \frac{\partial n}{\partial t} = \delta \frac{\partial^2 n}{\partial x^2} + n^2 w - n, \\ 0 = \frac{\partial^2 w}{\partial x^2} + a - w - n^2 w. \end{cases} \tag{2.5}$$

First we solve for the steady states of the corresponding ODE systems, which satisfy

$$\begin{cases} n_t = -n + w n^2 = 0, \\ 0 = a - w - w n^2. \end{cases} \tag{2.6}$$

It is clear that for $a < a_c = 2$, there is only one spatially homogeneous steady state $n = 0, w = a$ and for $a > a_c = 2$ we have three steady states: $n = 0, w = a$ and

$$n_\pm = \frac{a \pm \sqrt{a^2 - 4}}{2}, w_\pm = \frac{1}{n_\pm}. \tag{2.7}$$

Separating w in the second equation in (2.6) and plugging into the first one we obtain that

$$n_t = -n + \frac{a n^2}{1 + n^2} = \frac{-n(n - n_+)(n - n_-)}{1 + n^2}. \tag{2.8}$$

From Figure 2.1 and Figure 2.2 we can see that 0 and n_+ are stable and n_- is unstable with respect to the ODE dynamics.

Next we linearize around n_+, w_+ in the PDE system (2.5), i.e., let $n = n_+ + e^{\lambda t} \cos(mx)\hat{\phi}$ and $w = w_+ + e^{\lambda t} \cos(mx)\hat{\psi}$, where $m = \frac{k\pi}{L}, k = 0, 1, 2...$ and $|\hat{\phi}|, |\hat{\psi}| \ll 1$. Then we obtain

$$\begin{cases} \lambda \hat{\phi} = (1 - \delta m^2)\hat{\phi} + n_+^2 \hat{\psi}, \\ 0 = -2\hat{\phi} - (m^2 + 1 + n_+^2)\hat{\psi}; \end{cases} \tag{2.9}$$

which can be simplified as one equation $\lambda \hat{\phi} = \left(1 - \delta m^2 - \frac{2n_+^2}{m^2 + 1 + n_+^2}\right)\hat{\phi}$. Thus

$$\lambda = 1 - \delta m^2 - \frac{2n_+^2}{m^2 + 1 + n_+^2}. \tag{2.10}$$

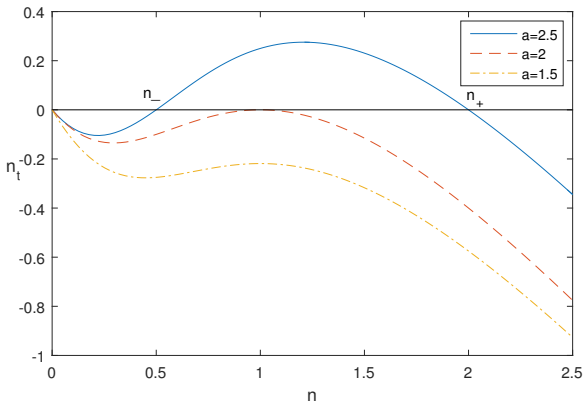

Figure 2.1: Evolution of n_t (2.8) with respect to n with different values of a.

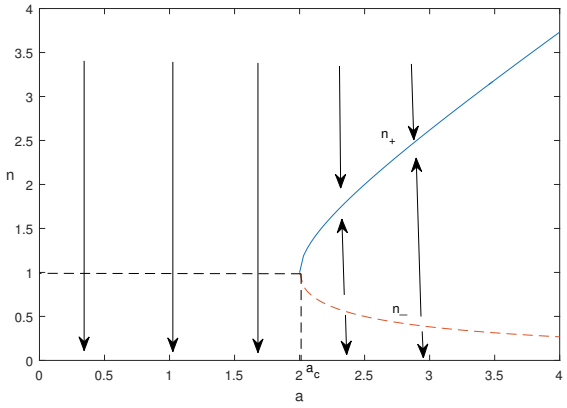

Figure 2.2: Evolution of vegetation n with respect to slow precipitation of a; the solid line denotes the steady state n_+, the dashed line denotes the steady state n_-.

Figure 2.3 shows how λ changes with respect to m with different values of parameter a. When $a = 2.7$, λ is always negative; when $a = 2.1$, there exists a unstable band $m \in (m_1, m_2)$. Turing bifurcation occurs when $\lambda = \frac{\partial \lambda}{\partial m} = 0$, thus the critical point at which Turing instability occurs is

$$a_p = \frac{3 - 2\sqrt{2 - 2\delta}}{\sqrt{(3 - 2\sqrt{2 - 2\delta} - \delta)\delta}}. \tag{2.11}$$

Hence the steady state n_+ undergoes a Turing instability to a patterned state at $a = a_p$, where a_p is express in (2.11).

Figure 2.4 illustrates the evolution of pattern formation induced from the stable steady state n_+, w_+ with some random perturbations. The parameters are $a = 2.1$, $\delta = 0.05$ and the initial condition is the homogenous steady state n_+ plus very small random perturbations. After some transient period, the solution is no longer homogenous and some patterns are formed, as shown at t = 500.

2.2 A brief review of delayed bifurcation

In this section we review delayed bifurcation phenomenon for ODE's. This analysis can also be applied to some PDEs when we reduce them to ODEs after linearization around the steady states. For example, we consider the following problem in the

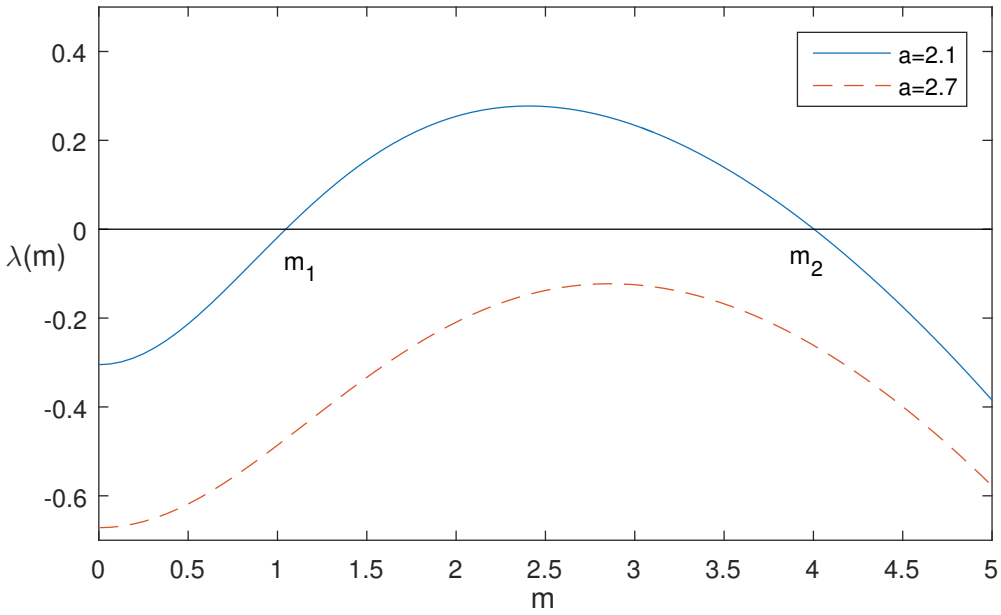

Figure 2.3: λ with respect to m with different values of a .

domain $(0, \pi)$:

$$\begin{cases} u_t = u_{xx} + a(\varepsilon t)u - u^3, \\ u(0,t) = u(\pi,t) = 0, \\ u(x,0) = 0, \end{cases} \tag{2.12}$$

where $a(\varepsilon t) = \varepsilon t$. The homogeneous steady state of (2.12) is $u = 0$. We linearize around $u = 0$, i.e., $u = 0 + \sum_{m=0}^{\infty} \phi_m(t)\sin(mx)$ with $|\phi_m| \ll 1$ and plug it in (2.12), then we obtain

$$\varepsilon\phi_s = (s - m^2)\phi + O(\phi^2), m = 1, 2...; \tag{2.13}$$

where $s = \varepsilon t$. This is a ODE problem which has been studied in [15] and [11]. Solving (2.13) under the assumption that $\phi(0) = \phi_0$ we obtain the exact solution

$$\phi = \phi_0 e^{\frac{1}{\varepsilon}(\frac{s^2}{2} - m^2 s)}, \quad m = 1, 2 \ldots. \tag{2.14}$$

Here we define the blow-up time s_b to be such that $\phi = \phi_0$. Alternatively, ϕ starts to grow rapidly at $s = s_b$. Solve for $\frac{s^2}{2} - m^2 s = 0$ yields $s = 0$ or $s = 2m^2$, since ϕ is decreasing in $(0, m^2)$, Thus the blow up time of ϕ is $s_b = \varepsilon t_b = \min(2m^2) = 2$. Note that ϕ starts to grow at $s = m^2$ but the growth is not observed until $s = 2m^2$, which is interpreted as delay in bifurcation.

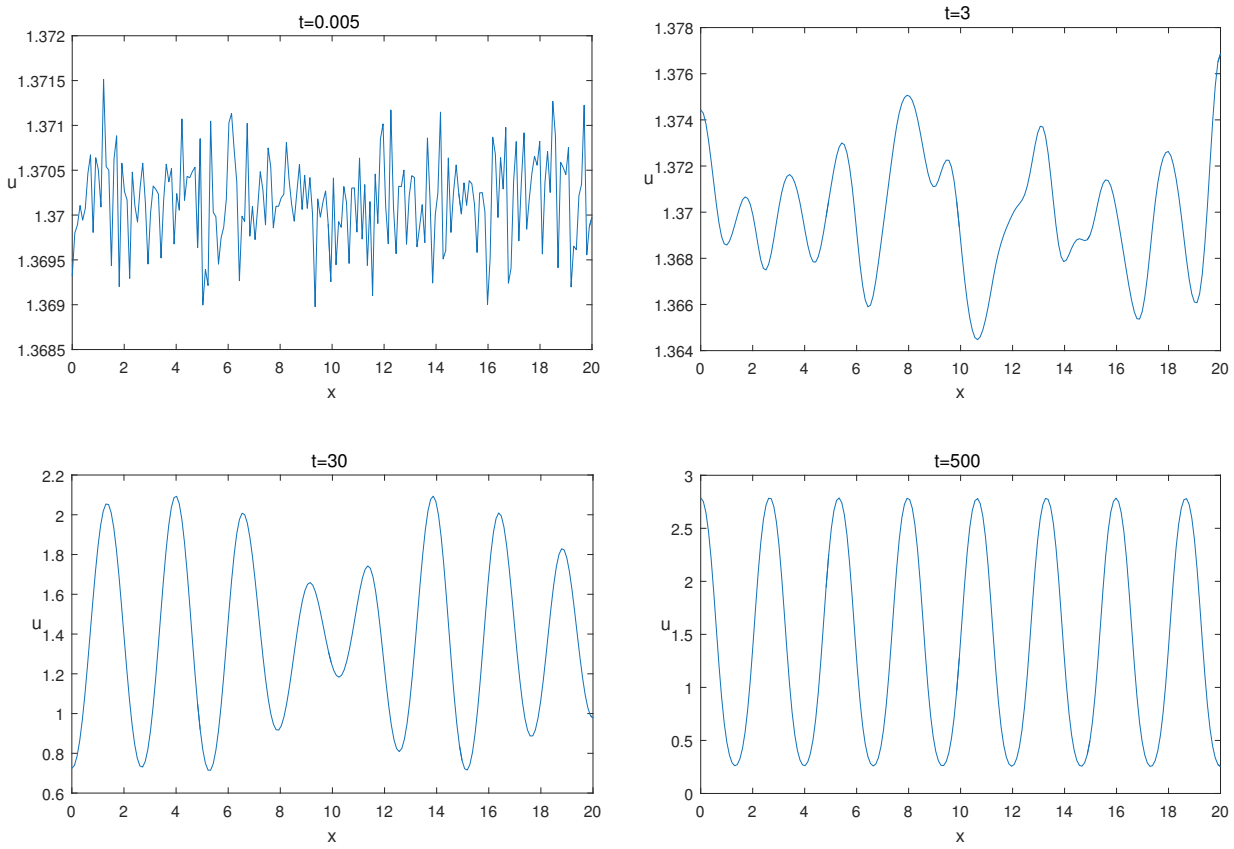

Figure 2.4: Example of Turing instability of Klausmeier model with $a = 2.1, \delta = 0.05$.

2.3 Fokker-Planck PDE

There is a wide range of situations including population dynamics, protein kinetics, turbulence, finance, and engineering that have non-deterministic dynamics, which can be described by stochastic differential equations (SDE). Since in stochastic differential equations one or more of the terms is a stochastic process, the solution is also a stochastic process. Moreover since most SDE are unsolvable analytically and to analyze properties of the stochastic process, it is important to get the density distribution of the solution. In statistical mechanics, the Fokker-Planck equation is a partial differential equation that describes the time evolution of the probability density function of the velocity of a particle under the influence of drag forces and random forces, as in Brownian motion. It was first used by Fokker [32] and Planck [33] to describe the Brownian motion of particles and is also known as the Kolmogorov forward equation (diffusion), named after Andrey Kolmogorov, who first introduced it in a 1931 paper

[34]. Suppose we have following SDE in one dimension:

$$dX_t = f(X_t, t)dt + \sigma(X_t, t)dW_t,$$

where dW_t denotes the standard Wiener process. Then the probability density $p(x, t)$ satisfies Fokker-Planck partial differential equation

$$\frac{\partial}{\partial t}p(x,t) = -\frac{\partial}{\partial x}\big(f(x,t)p(x,t)\big) + \frac{\partial^2}{\partial x^2}\big(D(x,t)p(x,t)\big), \tag{2.15}$$

where $f(x, t)$ denotes drift term and $D(x, t) = \frac{\sigma^2(X_t,t)}{2}$ is the diffusion coefficient.

2.3.1 Derivation of Fokker-Planck equation

The derivation of Fokker-Planck PDE and more details in this section can be found in [35], [36] and [37]. We first consider a one-dimensional Markov process $\{X(t) : t > 0\}$ satisfying

$$dX(x,t) = a(x,t)dt + b(x,t)dW,$$

where W is a standard Wiener Process. We use $P(x, s)$ to denote the probability that $X(s) = x$; moreover, we use $P(X(t) = y; X(s) = x)$ to denote the joint probability distribution, i.e. the probability that $X(t) = y$ and $X(s) = x$; and $P(y, t|x, s)$ to denote conditional (or transition) probability distribution, i.e., the probability that $X(t) = y$ given that $X(s) = x$, defined as $P(X(t) = y; X(s) = x) = P(y, t|x, s)P(x, s)$.

For any continuous state Markov process, the Chapman-Kolmogorov equation is satisfied, which is

$$P(X(t) = y|X(s) = x) = p(y,t|x,s) = \int p(y,t|z,\tau)p(z,\tau|x,s)dz, s < \tau < t. \tag{2.16}$$

This is the probability of going from x to y via z, "summed" over all possible intermediate z at time τ. To derive Fokker-planck equation, a partial differential equation for the time evolution of the transition probability density function, we first consider an integral

$$\int_{-\infty}^{\infty} g(y)\frac{\partial P(y,t|x,s)}{\partial t}dy,$$

where $g(y)$ is a smooth function. Writing

$$\frac{\partial P(y,t|x,s)}{\partial t} = \lim_{\Delta t \to 0}\frac{P(y,t+\Delta t|x,s) - P(y,t|x,s)}{\Delta t}, \tag{2.17}$$

and interchanging the limit with the integral, it follows that

$$\int_{-\infty}^{\infty} g(y)\frac{\partial P(y,t|x,s)}{\partial t}dy = \lim_{\Delta t\to 0}\int_{-\infty}^{\infty} g(y)\big(\frac{P(y,t+\Delta t|x,s)-P(y,t|x,s)}{\Delta t}\big)dy. \quad (2.18)$$

Applying the Chapman-Kolmogorov identity (2.16), the right hand side of (2.18) can be written as

$$\lim_{\Delta t\to 0}\frac{1}{\Delta t}\int_{-\infty}^{\infty} g(y)\int_{-\infty}^{\infty} P(y,t+\Delta t|z,t)P(z,t|x,s)dzdy - \int_{-\infty}^{\infty} g(y)P(y,t|x,s)dy. \quad (2.19)$$

Interchanging the limits of integration in the first term of (2.19), letting $y \to z$ in the second term, and using the identity $\int_{-\infty}^{\infty} P(y,t+\Delta t,z,t) = 1$, then (2.19) becomes

$$\lim_{\Delta t\to 0}\frac{1}{\Delta t}\int_{-\infty}^{\infty} P(z,t|x,s)\int_{-\infty}^{\infty} P(y,t+\Delta t|z,t)\big(g(y)-g(z)\big)dydz. \quad (2.20)$$

Taylor expanding $g(y)$ about z gives

$$\lim_{\Delta t\to 0}\frac{1}{\Delta t}\int_{-\infty}^{\infty} P(z,t|x,s)\int_{-\infty}^{\infty} P(y,t+\Delta t|z,t)\big((y-z)g'(z)+\frac{(y-z)^2}{2}g''^{3})\big)dydz. \quad (2.21)$$

Since $\lim_{\Delta t\to 0}\frac{1}{\Delta t}\int_{-\infty}^{\infty}(y-z)P(y,t+\Delta t|z,t)dy$ is the expectation of the process $X(t)$ and $\lim_{\Delta t\to 0}\frac{1}{\Delta t}\int_{-\infty}^{\infty}(y-z)^2P(y,t+\Delta t|z,t)dy$ is the variance of the process $X(t)$, we have

$$\lim_{\Delta t\to 0}\frac{1}{\Delta t}\int_{-\infty}^{\infty}(y-z)P(y,t+\Delta t|z,t)dy = \lim_{\Delta t\to 0}\frac{1}{\Delta t}E(X(t+\Delta t)-X(t)) = a(z,t), \quad (2.22)$$

$$\lim_{\Delta t\to 0}\frac{1}{\Delta t}\int_{-\infty}^{\infty}(y-z)^2P(y,t+\Delta t|z,t)dy = \lim_{\Delta t\to 0}\frac{1}{\Delta t}E\big((X(t+\Delta t)-X(t))^2\big) = b^2(z,t). \quad (2.23)$$

Substituting (2.22) and (2.23) into (2.21), we have

$$\int_{-\infty}^{\infty} g(y)\frac{\partial P(y,t|x,s)}{\partial t}dy = \int_{-\infty}^{\infty} P(z,t|x,s)\Big(a(z,t)g'(z)+\frac{b^2(z,t)}{2}g''(z)\Big)dz. \quad (2.24)$$

Integrating the RHS of (2.24) by parts yields

$$\begin{aligned}\int_{-\infty}^{\infty} g(y)\frac{\partial P(y,t|x,s)}{\partial t}dy &= g(z)a(z,t)P(z,t|x,s)\big|_{-\infty}^{\infty} - \int_{-\infty}^{\infty} g(z)\frac{\partial\big(a(z,t)P(z,t|x,s)\big)}{\partial z}dz\\ &\quad + g'(z)\frac{b^2(z,t)}{2}P(z,t|x,s)\big|_{-\infty}^{\infty} - g(z)\frac{\partial\Big(\frac{b^2(z,t)}{2}P(z,t|x,s)\Big)}{\partial y}\Big|_{-\infty}^{\infty}\\ &\quad + \int_{-\infty}^{\infty} g(z)\frac{\partial^2\big(\frac{b^2(z,t)}{2}P(z,t|x,s)\big)}{\partial z^2}dz \quad (2.25)\\ &= \int_{-\infty}^{\infty} g(z)\frac{\partial^2\big(\frac{b^2(z,t)}{2}P(z,t|x,s)\big)}{\partial z^2}dz - \int_{-\infty}^{\infty} g(z)\frac{\partial\big(a(z,t)P(z,t|x,s)\big)}{\partial z}dz,\end{aligned}$$

where at $z = \infty$ and $z = -\infty$, both the density function P and the derivatives of P go to 0. Thus we finally have

$$\frac{\partial}{\partial t}P(z,t|x,s) = -\frac{\partial}{\partial z}\big(a(z,t)P(z,t|x,s)\big) + \frac{\partial^2}{\partial z^2}\big(\frac{b^2(z,t)}{2}P(z,t|x,s)\big), \tag{2.26}$$

which is precisely the statement (2.15).

Chapter 3

The effect of spatio-temporal noise on the onset of Turing bifurcation

In this chapter we investigate the effect of small spatio-temporal noise on the onset of pattern formation for PDE's. The main mechanism responsible for the onset of patterns is due to a Turing instability. This instability amplifies any initial small spatial perturbation. A classical analysis of Turing instability concerns with computing parameter thresholds which initiate such an amplification. However it may take some time for the initial noise to fully develop into a Turing pattern. In this chapter we quantify this process, and in particular we compute the time it takes for the initial instability to grow fully, in the presence of spatio-temporal noise. The time it takes the instability to grow once the threshold is reached is referred to as a delay in the bifurcation.

We illustrate this theory on two examples. First, we consider a single cubic PDE which serves as a toy model for Turing instability. We then generalize our method to a system. In particular, we apply the method to Klausmeier model (1.3).

The results of this chapter are based on results in [1].

3.1 A single PDE

In this section, we consider the following single PDE with Dirichlet boundary condition in the 1-D domain $[0, \pi]$:

$$\begin{cases} u_t = u_{xx} + a(\varepsilon t)u - u^3 + noise \\ u(0,t) = u(\pi,t) = 0, \\ u(x,0) = 0, \end{cases} \tag{3.1}$$

where we take the spatio-temporal white noise to be

$$noise = \sigma_0 \sum_{m=0}^{\infty} \sqrt{dt}\xi_m(t)\sin(mx);$$

here σ_0 is the intensity of the noise and $\sqrt{dt}\xi_m(t)$ represents a time-dependent Wiener process; $\xi_m(t)$ is normally distributed with mean zero and variance one. Additionally, we assume that both the noise intesnity σ_0 and the drift speed ε are small:

$$\sigma_0 \ll 1, \quad \varepsilon \ll 1.$$

We first linearize $u(x,t) = 0 + \sum_{m=0}^{\infty} \phi_m(t)\sin(mx)$. Along each mode we then obtain

$$d\phi_m = (s - m^2)\phi_m dt + \sigma_0\sqrt{dt}\xi_m(t). \tag{3.2}$$

Note that when $s < m^2$, ϕ_m quickly decays and stays within a small interval of zero, regardless of the initial conditions. We will therefore assume, without loss of generality, that $\phi_m(0) = 0$.

The density distribution $\rho(\phi, s)$ for (3.2) satisfies the following Fokker-Planck equation:

$$\varepsilon\frac{\partial}{\partial s}\rho + (s - m^2)\frac{\partial}{\partial \phi_m}(\phi_m\rho) = \frac{\sigma_0^2}{2}\frac{\partial^2\rho}{\partial\phi_m^2}, \tag{3.3}$$

with initial condition $\phi(0) = 0$ corresponding to $\rho(\phi, 0) = \delta(\phi)$, where $\delta(\phi)$ is the Dirac delta function.

By doing the following change of variables,

$$\xi = \phi\exp\left(-\frac{s^2 - 2m^2 s}{2\varepsilon}\right), \quad S = \frac{\sigma_0^2}{2\varepsilon}\int_0^s \exp\left(-\frac{\hat{s}^2 - 2m^2\hat{s}}{\varepsilon}\right)d\hat{s},$$

$$\text{and} \quad \rho(\phi, s) = \exp\left(-\frac{1}{\varepsilon}\int_0^s (\frac{\tau^2}{2} - m^2\tau)d\tau\right)v(\xi, S),$$

equation (3.3) can be transformed into a standard diffusion equation $v_S = v_{\xi\xi}$ subject to initial condition $v(\xi, 0) = \delta(\xi)$. The solution for $v(\xi, S)$ is simply the fundamental solution of the diffusion equation $v(\xi, S) = \frac{1}{\sqrt{4\pi S}}\, e^{-\xi^2/(4S)}$. This yields the following explicit solution for $\rho(\phi, s)$,

$$\rho(\phi, s) = \frac{1}{\sqrt{2\pi}\sigma}e^{\frac{-\phi^2}{2\sigma^2}}, \tag{3.4}$$

where σ^2 is the variance of $\rho(\phi, s)$ given by

$$\begin{aligned}\sigma^2(s\,; m) &= 2S\exp\big(\frac{s^2 - 2m^2 s}{\varepsilon}\big) \\ &= \frac{\sigma_0^2}{\varepsilon}\int_0^s \exp\Big(\frac{s^2 - 2m^2 s - (\hat{s}^2 - 2m^2\hat{s})}{\varepsilon}\Big)d\hat{s}.\end{aligned} \tag{3.5}$$

Next we can approximate σ^2 using Laplace's method for rapidly decaying integrals. Recall [38] that the Laplace's method is the formula

$$\int_a^b f(x)e^{\frac{1}{\varepsilon}g(x)} \sim \sqrt{\frac{2\varepsilon\pi}{|g''(x_0)|}} f(x_0)e^{\frac{1}{\varepsilon}g(x_0)}, \tag{3.6}$$

where we assume that $g(x)$ is a twice differentiable function on $[a,b]$ and $x_0 \in [a,b]$ is the unique point such that $g(x_0) = \max_{[a,b]} g(x)$; in addition, we assume that $g''(x_0) < 0$.

Applying (3.6) to (3.5), we have $a = 0, b = s$, $f(x) = 1$ and $g(x) = -x^2 + 2m^2x + s^2 - 2m^2s$, thus $x_0 = m^2$ and $g''(x_0) = -2$. Assuming that $s > m^2$, we then obtain

$$\sigma(s;m) \sim \sigma_0(\frac{\pi}{\varepsilon})^{\frac{1}{4}} \exp\big(\frac{(s-m^2)^2}{2\varepsilon}\big). \tag{3.7}$$

Given any positive constant r, we now define the blow-up time s_0 to be the first time such that $|\phi(s)| = r$. The distribution of the blow up time is then given by

$$\begin{aligned} F(s) &= P\big(|\phi| > r\big) \\ &= \frac{2}{\sigma\sqrt{2\pi}} \int_r^\infty \exp(-\frac{\phi^2}{2\sigma^2}) d\phi, \end{aligned} \tag{3.8}$$

where $\sigma(s;m)$ is approximated by (3.7). Thus the density distribution of the blow up time s_b can be obtained by taking the derivative of $F(s)$

$$f(s) = F'(s) = \frac{2}{\sqrt{2\pi}\sigma^2} \exp(-\frac{r^2}{2\sigma^2}) \frac{d\sigma}{ds}, \quad (s > m^2). \tag{3.9}$$

Note that σ implicitly depends on m; so that each different mode m yields a different distribution of the blowup time. For the simple equation (3.1), the unstable modes $m = 1, 2, 3 \ldots$ are well-separated and the corresponding blowup distributions do not overlap except for exponentially small tail. Therefore the blowup of the mode $m = 1$ occurs before any other mode, and it is the one that is observed. As we will see in §3.2, this is no longer the case for more complex reaction-diffusion systems, and the various unstable modes can bunch up together and interact with each-other in a complicated way.

A simpler characterization of the blow-up time was proposed in [1]. Rather than looking at the whole distribution, we defined a single "take-off" point to be the time

at which the standard deviation σ starts to grow exponentially. This corresponds to setting $\sigma = 1$ in (3.7), resulting in

$$s_b = \min_m \left(\sqrt{-2\varepsilon \ln(\sigma_0 (\frac{\pi}{\varepsilon})^{\frac{1}{4}})} + m^2 \right) = \sqrt{-2\varepsilon \ln(\sigma_0 (\frac{\pi}{\varepsilon})^{\frac{1}{4}})} + 1. \tag{3.10}$$

The minimum is taken over all admissible modes m, in this case $m = 1, 2, \ldots$.

Note that the distribution (3.9) depends on an arbitrary parameter r; on the other hand the characterization (3.10) does not. In the next section we look at how well the formulas (3.9) and (3.10) perform when compared with full numerical simulations of the original model (3.1).

We now compare our density distribution (3.9) and the "take-off"point s_b (3.10) with numerical simulations of (3.1) obtained using MATLAB. To solve (3.1) numerically, we use finite differences method for the PDE, which we now describe.

Discretize in space using N gridpoints, $\Delta x = \frac{\pi}{N}$, and in time using stepsize Δt so that $u(x_k, t_j) \approx u_j^k$ where $x_k = k\Delta x$ with $k = 1, 2, ...N$, $t_j = j\Delta t$. To ensure numerical stability with a reasonably large time stepsize, we use a simple implicit-explicit Euler scheme as follows:

$$\frac{u_{j+1}^k - u_j^k}{\Delta t} = \frac{u_{j+1}^{k+1} + u_{j+1}^{k-1} - 2u_{j+1}^k}{(\Delta x)^2} + a(\varepsilon t_j) u_{j+1}^k - (u_j^k)^3 + \sigma_0 \frac{1}{\Delta t} dW_j^k. \tag{3.11}$$

Here dW_j^k is the discretization of the Wiener process. Care must be taken to truncate the infinite series to N modes to avoid oversampling,

$$dW_j^k = \sqrt{\Delta t} \sum_{m=0}^{N-1} \xi_m \sin(m x_k), \tag{3.12}$$

where ξ_m is a normal random variable of mean zero and variance 1. Alternatively, note from the definition (3.12) that dW_j^k is normally distributed (since it is a sum of normal variables), that its mean is zero and its variance is given by

$$\mathrm{var}(dW_j^k) = \Delta t \frac{N}{2}, \tag{3.13}$$

where $\xi_j(t_k)$ is a real Gaussian random variable. To derive (3.13), we used the fact that

$$\sum_{m=0}^{N-1} \sin^2(m x_k) = \sum_{m=0}^{N-1} \sin\left(\frac{mk\pi}{N}\right) = \frac{N}{2}.$$

For the numerical implementation, we therefore take $dW_j^k = \sqrt{\Delta t \frac{N}{2}} \times$ `randn`, where `randn` is the Matlab command which generates a normally distributed random number.

Figure 3.1 and 3.2 are plots with different values of drift speed ε, showing reasonable agreement between our density distribution by analysis and the histogram by simulations. We chose $r = 0.05$ and conducted 1000 full simulations of system (3.1) using the finite differences method described above to obtain the histogram. The solid curve denotes the density distribution of blow up time, and the red line denotes the "take-off" value (3.10). From these figures, we observe that as ε increases, both the mean and the variance of the blowup time increase as well. A larger choice of r results in a slight shift of the distributions to the right, with a better agreement with the vertical dashed line (3.10). However if r is chosen too large, the nonlinear term u^3 in (3.1) is no longer negligible, so that the density distribution approximation (3.9) breaks down.

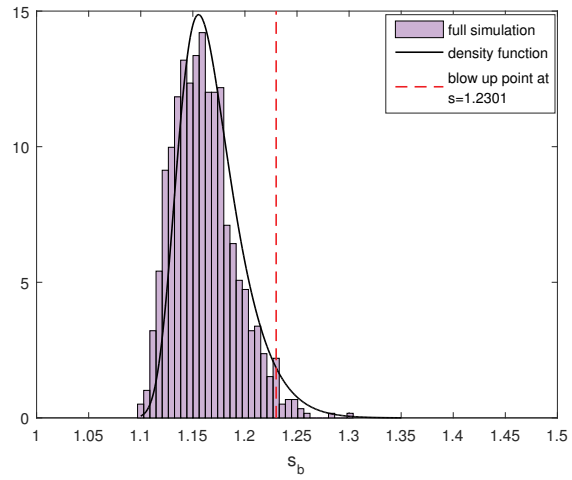

Figure 3.1: Numerical verification of density distribution of s_b with parameters $\varepsilon = 0.005, \sigma_0 = 0.001$ and $r = 0.05$, the mean of s_b is 1.175 and variance is 0.1105;

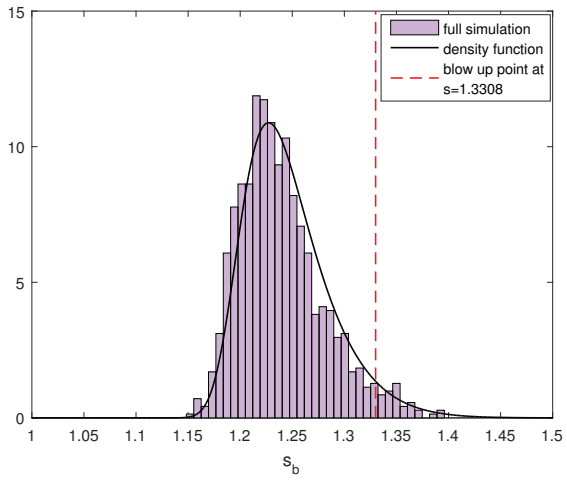

Figure 3.2: Numerical verification of density distribution of s_b with $\varepsilon = 0.01, \sigma_0 = 0.001$ and $r = 0.05$, the mean of s_b is 1.2459 and variance is 0.1444.

3.2 Klausmeier model with $b = 0$ and $c = 0$

In this section, we consider a modified version of Klausmeier model with Neumann boundary condition in the domain $[0, L]$ with the assumption that $b = 0, c = 0$. The

results in this section were previously published in [1].

Scaling $d = 1$ results in the following equations:

$$\begin{cases} \frac{\partial n}{\partial t} = \delta \frac{\partial^2 n}{\partial x^2} + n^2 w - n, \\ 0 = \frac{\partial^2 w}{\partial x^2} + a(\varepsilon t) - w - n^2 w + noise. \end{cases} \tag{3.14}$$

As in system (3.1), we take the spatio-temporal white noise to be

$$noise = \sigma_0 \sum_m \sqrt{dt} \xi_m(t) \cos(mx);$$

we used the cosine series here instead of sine since the boundary conditions are now Neumann; the sum is taken over all modes $m = k\pi/L$, $k = 0, 1, 2, \ldots$. The precipitation $a(\varepsilon t)$ is assumed to be slowly decreasing with ε controlling the speed of the decrease... Note that the steady state n_+ doesn't exist when a is below the fold point $a_c = 2$.

For concreteness, in the numerical simulations below we take

$$a(\varepsilon t) = a_0 - \varepsilon t, \tag{3.15}$$

where a_0 is assumed to be above the Turing threshold $a_p = \frac{3-2\sqrt{2-2\delta}}{\sqrt{(3-2\sqrt{2-2\delta}-\delta)\delta}}$. However we give the theory for a general function $a(\varepsilon t)$. The precise form of $a(\varepsilon t)$ is not important as long as $a_0 = a(0)$ is above a_p and a decreases below a_p with time.

We already conducted the stability analysis for the stable steady state n_+, w_+ from (2.7) in §2.1. When a is replaced by $a = a(\varepsilon t)$, we obtain the following quasi-steady states:

$$n_\pm(\varepsilon t) = \frac{a(\varepsilon t) \pm \sqrt{a^2(\varepsilon t) - 4}}{2}, \quad w_\pm(\varepsilon t) = \frac{1}{n_\pm(\varepsilon t)}. \tag{3.16}$$

Linearizing near n_+, w_+, we write

$$n(x,t) = n_+(\varepsilon t) + \phi(x,t), \quad w(x,t) = w_+(\varepsilon t) + \psi(x,t),$$

where $|\phi|, |\psi| \ll 1$ to obtain

$$\begin{cases} \frac{d\phi}{dt} + \varepsilon n_+'(\varepsilon t) = \delta \frac{d^2\phi}{dx^2} + \phi + n_+^2(\varepsilon t)\psi, \\ 0 = (\frac{d^2\psi}{dx^2} + (-1 - n_+^2(\varepsilon t))\psi - 2\phi)dt + \sigma_0 dW_t. \end{cases} \tag{3.17}$$

Separating variables in space, we let $\phi(x,t) = \sum \phi_m(t) \cos(mx)$ and $\psi(x,t) = \sum \psi_m(t) \cos(mx)$ to obtain

$$\begin{cases} \frac{d\phi_m}{dt} = -m^2 \delta \phi_m + \phi_m + n_+^2 \psi_m, \\ 0 = (-m^2 \psi_m + (-1 - n_+^2)\psi_m - 2\phi_m)dt + \sigma_0 \sqrt{dt} \xi_m(t). \end{cases} \tag{3.18}$$

Solving for ψ_m in the second equation in (3.18) and substituting in the first one, we have

$$d\phi_m = \alpha(\varepsilon t)\phi_m dt + \beta(\varepsilon t)dW_t, \quad \phi(0) = 0; \tag{3.19}$$

where

$$\alpha(\varepsilon t) = -m^2\delta + 1 - \frac{2n_+^2(\varepsilon t)}{m^2 + 1 + n_+^2(\varepsilon t)}, \quad \beta(\varepsilon t) = \frac{\sigma_0 n_+^2(\varepsilon t)}{m^2 + 1 + n_+^2(\varepsilon t)}. \tag{3.20}$$

Recall that the steady state n_+ undergoes Turing bifurcation at $a = a_p$ given by (2.11) when there is no noise and slow parameter ε. However, the slow drift and noise term have a combined effect which induce a delay in the bifurcation. To compute this delay, we proceed similarly to §3.1 by studying the density distribution $\rho(\phi, s)$ associated with (3.19). The density function $\rho(\phi, s)$ satisfies the following Fokker-Planck PDE

$$\varepsilon\frac{\partial}{\partial s}\rho + \alpha(s)\frac{\partial}{\partial\phi}(\phi\rho) = \frac{\beta^2(s)}{2}\frac{\partial^2\rho}{\partial\phi^2} \tag{3.21}$$

with initial condition $\phi(0) = 0$ in (3.21) corresponding to $\rho(\phi, 0) = \delta(\phi)$, where $\delta(\phi)$ is the Dirac delta function and s denotes the slow time εt.

Similar to §3.1, we first do the following change of variables

$$\hat{\xi} = \phi\exp\left(-\frac{1}{\varepsilon}\int_0^s \alpha(\tau)d\tau\right), \hat{S} = \int_0^s \frac{\beta^2(\hat{s})}{2\varepsilon}\exp\left(-\frac{2}{\varepsilon}\int_0^{\hat{s}} \alpha(\tau)d\tau\right)d\hat{s},$$

and

$$\rho(\phi, t) = \exp\left(-\frac{1}{\varepsilon}\int_0^s \alpha(\tau)d\tau\right)v(\xi, S)$$

to obtain the solution

$$\rho(\phi, s) = \frac{1}{\sqrt{2\pi}\hat{\sigma}}e^{\frac{-\phi^2}{2\hat{\sigma}^2}}, \tag{3.22}$$

where $\hat{\sigma}^2$ is the variance of ρ given by

$$\hat{\sigma}^2(s\,; m) = \int_0^s \beta^2(\tau)\exp\left(-\frac{2}{\varepsilon}\int_\tau^s \alpha(\tau)d\tau\right)d\tau. \tag{3.23}$$

Let s_p be the such that that $\alpha(s_p) = 0$. Applying Laplace's method from (3.6), for $s > s_p$, we obtain

$$\hat{\sigma}(s; m) \sim \exp\left(\frac{1}{\varepsilon}\int_{s_p}^s \alpha(\tau)d\tau\right)\beta(s_p)\left(\frac{\pi}{\varepsilon\alpha'(s_p)}\right)^{1/4},$$

where the dependence of $\hat{\sigma}$ on m is through that of α and β in (3.20). As in §3.1, we now define the "take-off" time $s_d = s_d(m)$ for the mode m to be such that $\sigma(s_d; m) =$

1. Note that s_d is such that $\sigma \ll 1$ when $s < s_d$ and $\sigma \gg 1$ when $s > s_d$. For a fixed mode m, the value of s_d is therefore found by solving simultaneously

$$\alpha(s_p) = 0; \tag{3.24}$$

$$\int_{s_p}^{s_d} \alpha(s)ds + \varepsilon \ln\left(\beta(s_p)\left(\frac{\pi}{\varepsilon\alpha'(s_p)}\right)^{1/4}\right) = 0. \tag{3.25}$$

Note that, depending on the parameters, a solution for s_d in (3.24) may not exist, in which case the corresponding mode m is never activated.

The first mode that gets activated yields the delayed "take-off" value for a:

$$a_d \equiv a(\min_m s_d(m)), \tag{3.26}$$

where the minimum is taken over all admissible modes m. These are the modes for which the solution to the system (3.24) exists. If no such modes exist, no "take-off" value of a exists, and the patterned state is never activated.

We now give numerical verification of a_d with different values of ε as given in (3.26) for system (3.15). The slow drift is taken to be $a = a_0 - \varepsilon t$ with $a_0 = 3$, $\sigma_0 = 0.0001, L = 20$ and $\delta = 0.05$. Figure 3.3 compares the analytic prediction for a_d and the delayed value $a_{d,num}$ as observed from direct numerical simulations of (3.14). To estimate a_d from direct simulations, we first define the blow up time $t_{d,num}$ at which $(\max_x n - \min_x n)/mean_x(n)$ first exceeds 1. We then calculate $a_{d,num} = a(\varepsilon t_{d,num})$. In Figure 3.3 we plot both the numerically computed $a_{d,num}$ the theoretical predictions for a_d given by (3.26). Good agreement is observed, at least for $a_d > 2$.

The theoretical prediction (3.26) for a_d ends at $a = 2$, which is the fold point of the homogeneous steady state (see Figure 2.2). However, we can see that for the values of $\varepsilon \in (0.01, 0.015)$, full numerical simulations show that homogeneous quasi-state jumps to the patterned state branch even when a has been decreased to *below* the fold point $a = 2$ where the homogeneous steady state n_+ no longer exists. This is due to the presence of slow relaxation dynamics: it is well known (see for example [38], §6.5) that there is a boundary layer of $O(\varepsilon^{1/3})$ near the fold point, so that the homogeneous state "falls off" not exactly at the fold point, but within $O(\varepsilon^{1/3})$ of it. This delay is readily apparent in Figure 3.3, where the numerics and asymptotics diverge near $a = a_c = 2$. To better capture this behaviour (and thus to better approximate the values of ε for which the extinction is observed), we replace the quasi-steady state approximation

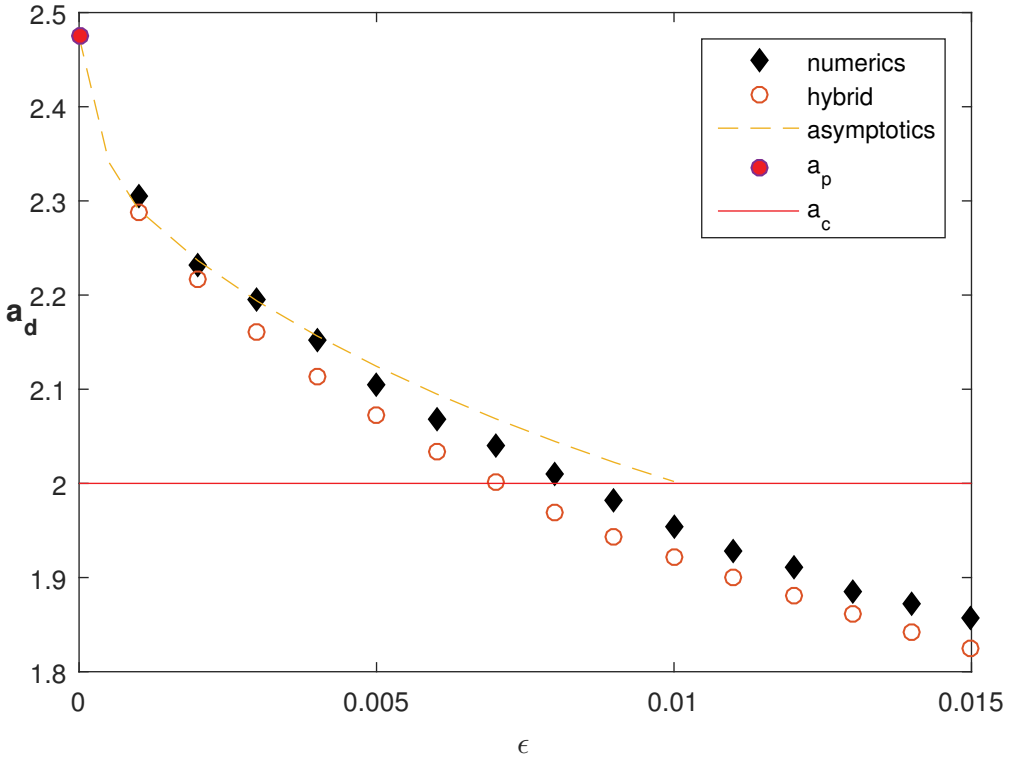

Figure 3.3: Comparison of asymptotic and full numerical results for a_d.

n_+ and w_+ in (3.16) by the solution to the homogeneous (ODE) system with a slowly changing

$$n_t = -n + n^2 w, 0 = a(\varepsilon t) - w - wn^2.$$

Moreover, it is no longer true that $n_+ w_+ = 1$ so that α, β in (3.20) are replaced by

$$\alpha(s) = -m^2\delta + (2nw - 1) - \frac{2n^2(s)}{m^2 + 1 + n^2(s)}, \tag{3.27}$$

$$\beta(s) = \frac{\sigma_0 n^2(s)}{m^2 + 1 + n^2(s)}. \tag{3.28}$$

With this modification, the computation for a_d is carried out as in before. This allowed us to better capture the transition to the patterned state even a is slightly below the tipping point $a = a_c$. This is clearly shown in the curve labelled "hybrid" and its agreement with the full numerical result in Figure 3.3.

Figure 3.4 shows the evolution of $\max(n)$ for four different values of ε. It can be observed that for bigger ε, we have smaller "take-off" value a_d; when ε is too

large, there is no "take-off" value exists, and the patterned state is never activated. Moreover, we can see two simulations for $\varepsilon = 0.004$ from Figure 3.4, and each with different random seeds. The bunching together of "take-off" points for different simulations when $\varepsilon = 0.004$ illustrates that a_d is insensitive to the particular random seeds chosen.

We also give the simulation of "take off" value a_d with different value of diffusion coefficient δ and noise σ_0. Figure 3.5 shows how the "take off" value a_d changes with respect to δ. It can be observed that for greater δ, we have smaller "take off" value. Figure 3.6 shows the effect of different size of noise to the "take off" value a_d. We can see that larger noise makes better resilience of a homogeneous state against tipping points.

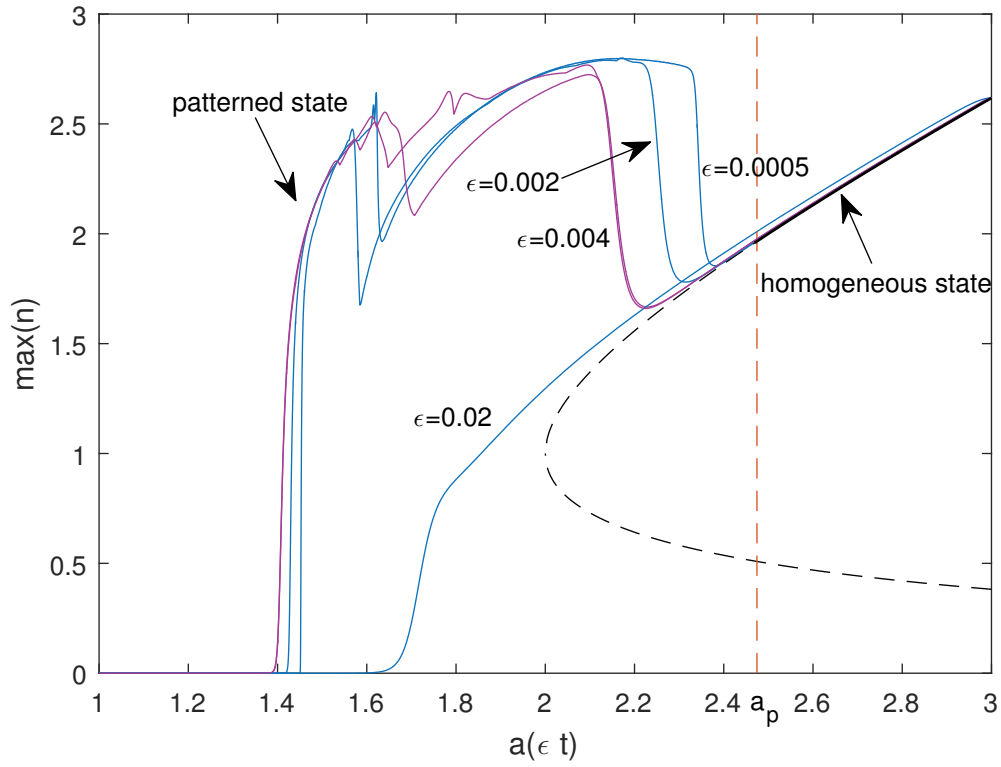

Figure 3.4: The evolution of max n as a function of a with ε as indicated. The dashed line shows a_d as given by (3.26). The black solid curve shows the homogeneous steady state. The curves denote simulations for four different values of ε each with different random seeds. The bunching together of take-off points for $\varepsilon = 0.004$ illustrates that a_d is insensitive to the particular seed chosen.

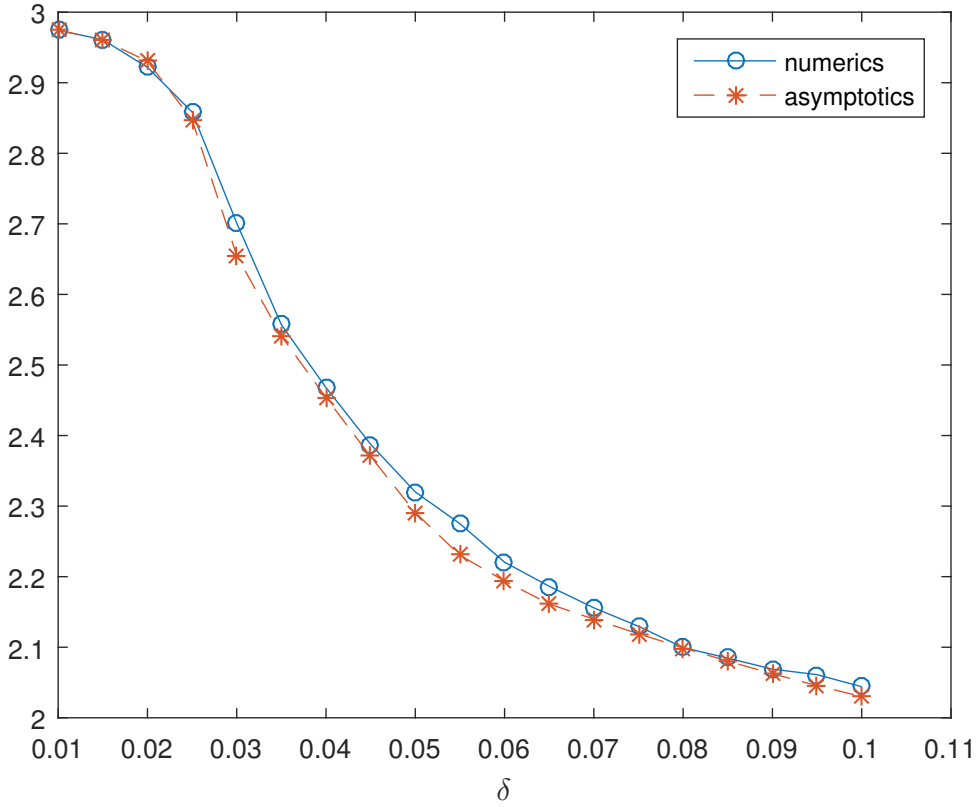

Figure 3.5: Comparison of asymptotic and full numerical results of a_d with different value of diffusion coefficient of vegetation δ. The other parameters are $\varepsilon = 0.001$, $\sigma_0 = 0.0001$ and $b = c = 0$.

3.3 Klausmeier model with $b \neq 0$ and $c = 0$

We now extend the analysis from [1] to consider the case where b is nonzero. As before, we set $d = 1$ and $c = 0$ in (1.3) resulting in

$$\begin{cases} \frac{\partial n}{\partial t} = \delta \frac{\partial^2 n}{\partial x^2} + n^2 w - n, \\ b\frac{\partial w}{\partial t} = \frac{\partial^2 w}{\partial x^2} + a(\varepsilon t) - w - n^2 w + \sigma_0 \frac{dW}{dt}, \\ dW = \sum_m \sqrt{dt}\xi_m(t)\cos(mx). \end{cases} \tag{3.29}$$

Linearizing around the homogeneous steady state $n = n_+ + \phi(x,t)$, $w = w_+ + \psi(x,t)$, where $|\phi(x,t)|, |\psi(x,t)| \ll 1$ yields the system

$$\begin{cases} \frac{\partial \phi}{\partial t} = \delta \frac{\partial^2 \phi}{\partial x^2} + n_+^2 \psi + \phi, \\ b\frac{\partial \psi}{\partial t} = \frac{\partial^2 \psi}{\partial x^2} - 2\phi - (1 + n_+^2)\psi + \sigma_0 \sum_m \frac{\sqrt{dt}}{dt}\xi_m(t)\cos(mx), \end{cases} \tag{3.30}$$

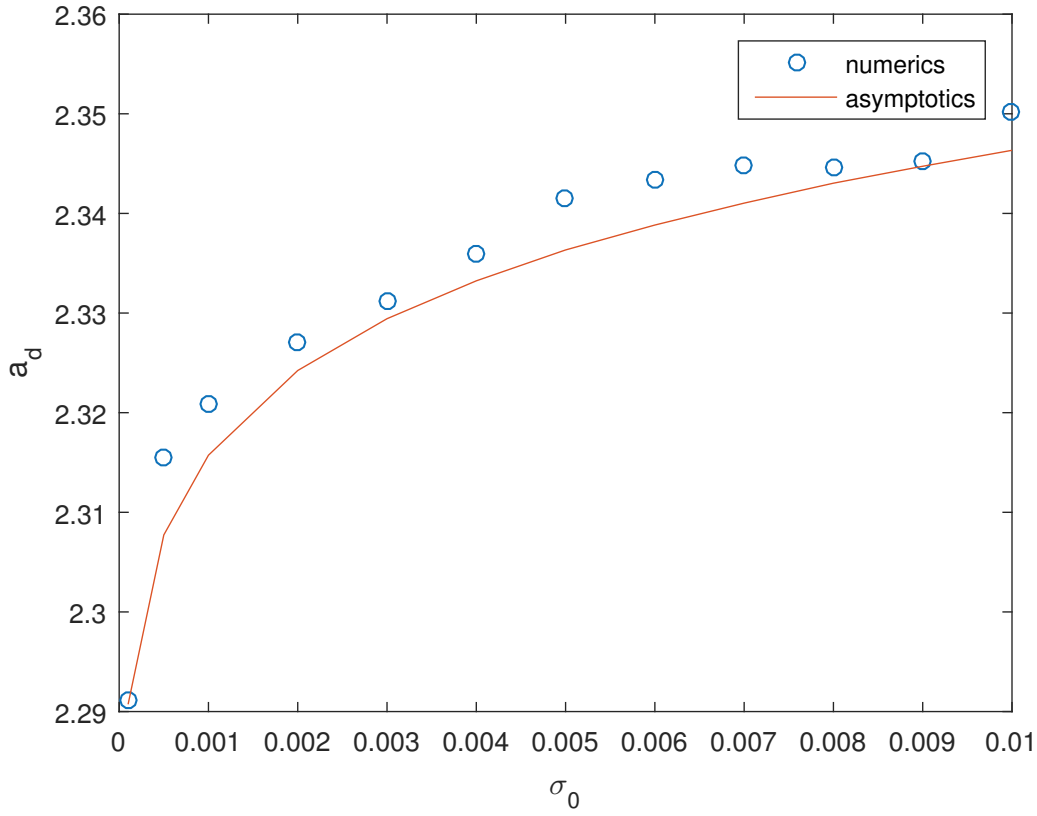

Figure 3.6: Comparison of asymptotic and full numerical results of a_d with different value of noise intensity σ_0. The other parameters are $\varepsilon = 0.001$, $\delta = 0.05$ and $b = c = 0$.

which can be written as function of slow time s

$$\begin{cases} \varepsilon \frac{\partial \phi}{\partial s} = \delta \frac{\partial^2 \phi}{\partial x^2} + n_+^2 \psi + \phi, \\ \varepsilon \frac{\partial \psi}{\partial s} = \frac{1}{b} \frac{\partial^2 \psi}{\partial x^2} - \frac{2}{b} \phi - \frac{1+n_+^2}{b} \psi + \frac{\sigma_0 \sqrt{\varepsilon}}{b} \sum_m \frac{\sqrt{ds}}{ds} \xi_m(t) \cos(mx). \end{cases} \tag{3.31}$$

Using separation of variables

$$\phi(x,t) = \sum_m \cos(mx)\, \phi_m(t); \quad \psi(x,t) = \sum_m \cos(mx)\, \psi_m(t);$$

the resulting system can be written as

$$\varepsilon Y_s = AY + F(s), \tag{3.32}$$

where

$$Y = \begin{pmatrix} \phi_m \\ \psi_m \end{pmatrix}, \quad A = \begin{pmatrix} -\delta m^2 + 1 & n_+^2(s) \\ -\frac{2}{b} & -\frac{m^2+1+n_+^2(s)}{b} \end{pmatrix}, \quad F(s) = \begin{pmatrix} 0 \\ \frac{\sigma_0}{b} \frac{\sqrt{\varepsilon}\sqrt{ds}\xi_m(t)}{ds} \end{pmatrix}. \tag{3.33}$$

To get the scalar form similar to (3.19), we use a WKB-type anzatz which we now describe. Multiply (3.32) by $W(s)$, where W satisfies $WA = \lambda W$. That is, W is the *adjoint* eigenvector corresponding to the eigenvalue $\lambda(s)$ of $A(s)$. Then system (3.32) becomes

$$\begin{aligned} \varepsilon W Y_s &= WAY + W\vec{F}(s) \\ &= \lambda WY + WF(s). \end{aligned} \tag{3.34}$$

Let $X = W(s)Y(s)$, then we have

$$X_s = \varepsilon W_s Y + WY_s \sim WY_s.$$

Thus at the leading order, (3.32) becomes

$$\varepsilon X_s \sim \lambda X + WF. \tag{3.35}$$

Since this equation is precisely of the form (3.19) with

$$\alpha(s) = \lambda; \quad \beta(s) = WF.$$

From here on, the analysis of §3.3 proceeds as before, and the take-off time is given by the same formula (3.24) except the formulas for α and β are more involved.

The equation for α satisfies

$$\alpha^2 + B\alpha + C = 0, \tag{3.36}$$

where

$$\begin{aligned} B &= -trace(A) = \frac{m^2 + 1 + n_+^2(s)}{b} + \delta m^2 - 1; \\ C &= \det(A) = (\delta m^2 - 1)\Big(\frac{m^2 + 1 + n_+^2(s)}{b}\Big) + \frac{2n_+^2(s)}{b}. \end{aligned}$$

In general, α can be complex; we treat an example of such a case in the subsequent §3.4. Furthermore, as b is increased, the homogeneous steady state undergoes a Hopf bifurcation when $B = 0$. For the purposes of this section, we only look at the regimes where α is purely real to avoid dealing with oscillatory behaviour.

There are two possible values for $\alpha(s)$ that must be considered: $\alpha_\pm = \frac{-B \pm \sqrt{B^2 - 4C}}{2}$. It turns out that α_- is always negative; the only relevant eigenvalue which is responsible for Turing instability is

$$\alpha(s) = \frac{-B + \sqrt{B^2 - 4C}}{2}. \tag{3.37}$$

The corresponding β is given by

$$\beta = \frac{\sigma_0}{\sqrt{\frac{4}{(\lambda+\delta m^2-1)^2} + b^2}}. \tag{3.38}$$

With these values, we evaluate a_d using (3.26). The integrals are all evaluated numerically using Matlab.

Figure 3.7 is the full simulation of the "take off" time a_d with different value of b. It's observed that for greater b, we have greater a_d.

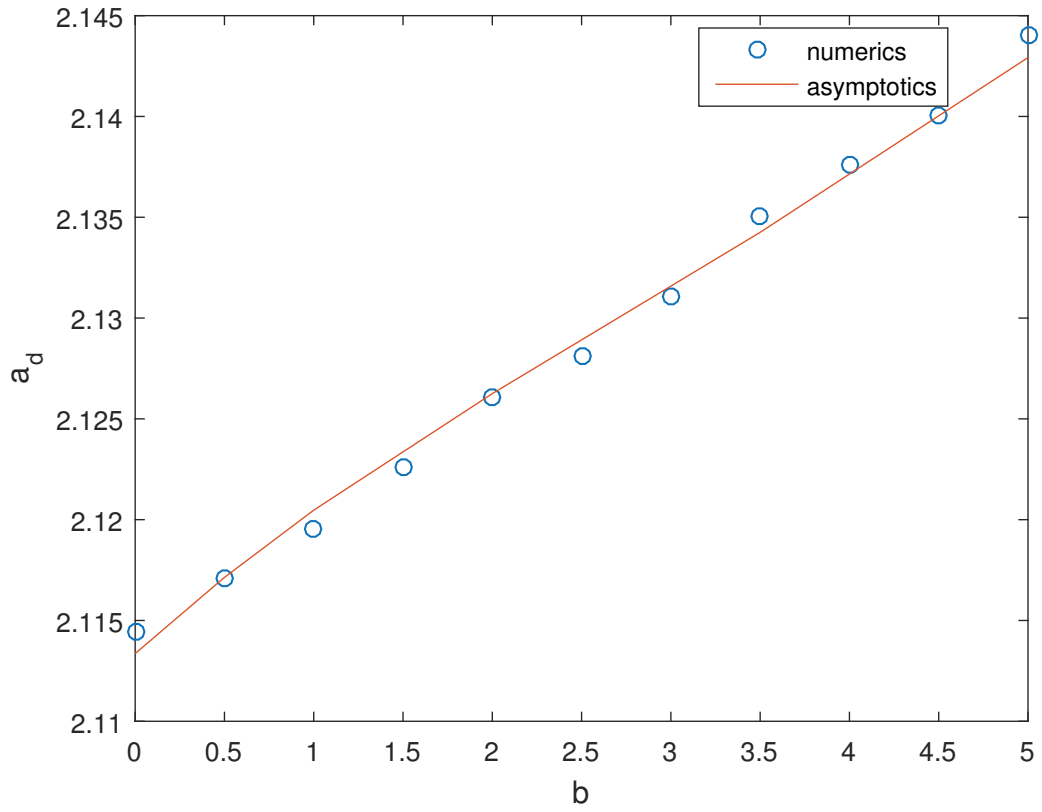

Figure 3.7: Comparison of asymptotic and full numerical results of a_d with different value of parameter b. The other parameters are $\varepsilon = 0.005$, $\delta = 0.05$ and $\sigma_0 = 0.0001$.

In the limit $b \to 0$, we recover the results of §3.2. To see this, we expand α for small b as $\alpha = \alpha_0 + b\alpha_1 + \ldots$; substituting this expansion into (3.36) and collecting the powers of b yields

$$\left(\frac{m^2+1+n_+^2}{b}\right)\alpha_0 + (\delta m^2 - 1)(\frac{m^2+1+n_+^2}{b}) + \frac{2n_+^2}{b} + O(1) = 0;$$

solving for α_0 then recovers the formula (3.27). Similarly, the formula (3.28) is obtained by taking the limit of (3.38) as $b \to 0$.

Note that b cannot be too large since the simulation shows that large b may trigger Hopf bifurcation and the condition for Hopf bifurcation is that

$$B = \frac{m^2 + 1 + n_+^2(s)}{b} + \delta m^2 - 1 = 0, C = (\delta m^2 - 1)\Big(\frac{m^2 + 1 + n_+^2(s)}{b}\Big) + \frac{2n_+^2(s)}{b} > 0,$$

which yields that for some m and s, Hopf bifurcation happens when b satisfies the following condition

$$b = \frac{m^2 + 1 + n_+^2}{1 - \delta m^2} > 0 \quad \text{and} \quad 2n_+^2 > (1 - \delta m^2)(m^2 + 1 + n_+^2). \tag{3.39}$$

Note that for $m = 0$ mode, the second equation in (3.39) simplifies to $n_+ > 1$ which is always the case (see (2.7)). The first equation in (3.39) then becomes

$$b_{hopf} = 1 + n_+^2.$$

Our analysis above implicitly assumes that $b < b_{hopf}$.

3.4 Klausmeier model with $b = 0$ and $c \neq 0$

In this section we consider the case where $c \neq 0$. As before, we set $d = 1$ and $b = 0$ in (1.3) resulting in

$$\begin{cases} \frac{\partial n}{\partial t} = \delta \frac{\partial^2 n}{\partial x^2} + n^2 w - n, \\ 0 = \frac{\partial^2 w}{\partial x^2} + c\frac{\partial w}{\partial x} + a - w - n^2 w + \sigma_0 \frac{dW}{dt}; \end{cases} \tag{3.40}$$

where $dW = \sigma_0 \sum_m \sqrt{dt}\xi_m(t)\exp(imx)$. Because of the non-zero drift, for simplicity we consider periodic boundary conditions here, $n(0,t) = n(L,t)$ and $w(0,t) = w(L,t)$.

After linearization around n_+, w_+ with $n = n_+ + \phi(x,t), w = w_+ + \psi(x,t)$, we obtain the following system

$$\begin{cases} \phi_t = \delta\phi_{xx} + \phi + n_+^2\phi, \\ 0 = \psi_{xx} + c\psi_x - 2\phi - (1 + n_+^2)\psi + \sigma_0 \frac{dW_t}{dt}. \end{cases} \tag{3.41}$$

Separating ϕ and ψ in space and time, i.e., $\phi = \sum_0^m \phi_m(t)\exp(imx)$ and $\psi = \sum_0^m \psi_m(t)\exp(imx)$, and substituting them into (3.41) yields

$$\begin{cases} \phi_{mt} = (1 - \delta m^2)\phi_m + n_+^2\psi_m, \\ 0 = (icm - m^2)\psi_m - 2\phi_m - (1 + n_+^2)\psi_m + \sigma_0 \frac{\sqrt{dt}\xi}{dt}. \end{cases} \tag{3.42}$$

Solving for ψ in the second equation in (3.42) and plug it in the first one we obtain

$$d\phi = \tilde{\alpha}(\varepsilon t)\phi dt + \tilde{\beta}(\varepsilon t)dW_t, \tag{3.43}$$

where

$$\tilde{\alpha}(\varepsilon t) = -m^2\delta + 1 - \frac{2n_+^2(\varepsilon t)}{m^2 + 1 + n_+^2(\varepsilon t) - icm}; \tag{3.44}$$

$$\tilde{\beta}(\varepsilon t) = \frac{\sigma_0 n_+^2(\varepsilon t)}{m^2 + 1 + n_+^2(\varepsilon t) - icm}. \tag{3.45}$$

From (3.44) and (3.45) we can see that when we include parameter c, the eigenvalues are complex, thus we need to find its real part to determine the stability of steady states, which are

$$Re(\tilde{\alpha}(\varepsilon t)) = -m^2\delta + 1 - \frac{2n_+^2(\varepsilon t)(m^2 + 1 + n_+^2(\varepsilon t))}{\left(m^2 + 1 + n_+^2(\varepsilon t)\right)^2 + c^2m^2}; \tag{3.46}$$

$$Re(\tilde{\beta}(\varepsilon t)) = \frac{\sigma_0 n_+^2(\varepsilon t)(m^2 + 1 + n_+^2(\varepsilon t))}{\left(m^2 + 1 + n_+^2(\varepsilon t)\right)^2 + c^2m^2}. \tag{3.47}$$

From here on, the analysis of §3.4 proceeds as in §3.2, and the take-off time is given by the same formula (3.24) except the formulas for α and β are replaced by $Re(\tilde{\alpha}(\varepsilon t))$ and $Re(\tilde{\beta}(\varepsilon t))$.

In Figure 3.8 we compare our "take off" value a_d between direct simulations and asymptotic simulations. In the figure a good agreement can be observed, and with greater c, the solution will take off more earlier.

3.5 Conclusions

In this chapter we have studied the effect of spatio-temporal noise on the delay in the Turing bifurcation, following [1]. The main idea is to decompose the PDE dynamics along its Fourier modes, resulting in a decoupled infinite system of stochastic ODE's. Each SODE is an Ornstein-Uhlenbeck process, and we then use its associated density to study the blowup behaviour.

We have extended the work in [1] to incorporate a more general case of reaction diffusion systems (where $b \neq 0$ in §3.3), as well as to the case where there is a drift ($c \neq 0$ in §3.4) which results in complex eigenvalues. The former case required the use of adjoint eigenvector to reduce the system of stochastic ODE's to a single Ornstein-Uhlenbeck process.

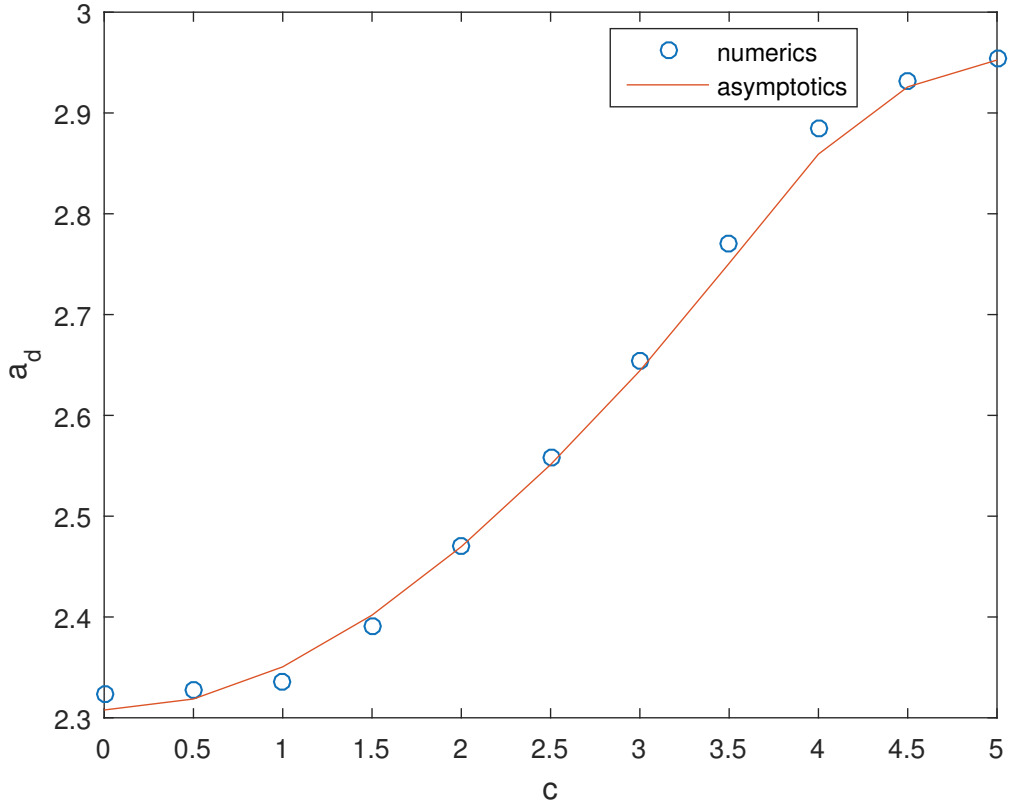

Figure 3.8: Comparison of asymptotic and full numerical results of a_d with different value of parameter c. The other parameters are $b = 0$, $\varepsilon = 0.005$, $\delta = 0.05$ and $\sigma_0 = 0.0005$.

In [1], the blow-up time is defined in terms of a blowup of the variance of the associated SODE's, and an asymptotic formula (3.24, 3.25) was given for this time. In reality, however, the blow-up times constitute a *density distribution*, and not a single number. In this chapter we have computed this distribution directly for the case of a single PDE (3.1). We used direct numerical simulations to validate our results. Unfortunately, these techniques do not work well for the Klausmeier model. We think that this is because the unstable modes in the Klausmeier model are clustered together and interact; there is no single mode that dominates, unlike the single PDE model (3.1), where the mode $m = 1$ becomes unstable well before any other. We are currently looking at extending our methods to examine how mode interaction affects the distribution of the blowup times.

Chapter 4

The effect of purely spatial noise on the onset of Turing bifurcation

In this chapter we will consider the case where the noise is no longer spatio-temporal noise, but replaced by purely spatial Gaussian white noise. Here we define the spatial noise as

$$noise = \sigma_0 \sum_{m=0}^{\infty} \xi_m \exp(imx); \tag{4.1}$$

where ξ_m is normally distributed and is independent of time with mean 0 and variance 1, and σ_0 is the noise intensity. Again we consider the examples from §3: a single PDE and the Klausmeier model. Similar to the analysis of §3.1, the main idea is to decompose the PDE dynamics into its Fourier modes. The difference here is that for each mode, rather than obtaining a stochastic ODE (the Ornstein-Uhlenbeck process), we obtain a *deterministic* linear ODE, but with random inhomogenuity. Based on the ODE, we compute the distribution of delays in the bifurcation. We then compare the results we get between spatio-temporal noise and purely spatial noise.

4.1 An ODE with random parameters

Let us first consider the following single ODE,

$$\phi_t = \alpha(\varepsilon t)\,\phi + \beta(\varepsilon t)\,\xi, \tag{4.2}$$

where ξ is chosen from a standard normal distribution. As in §3.1, we assume that

$$\beta \ll 1, \quad \varepsilon \ll 1$$

corresponds to low noise and slow parameter drift. We also assume that $\alpha(\varepsilon t)$ is an increasing function with $\alpha(0) < 0$, and with $\alpha(s_p) = 0$ for some $s_p > 0$. By making a change of variables $s = \varepsilon t$, this ODE is equivalent to

$$\varepsilon\phi_s = \alpha(s)\phi + \beta(s)\xi. \tag{4.3}$$

Since $\alpha(s)$ is initially negative, the solution decays at first, then starts to grow rapidly when $s > s_p$. Given a positive constant r, we thus define the blow-up time to be the first time $s_b > s_p$ such that $|\phi(s_b)| = r$. We wish to know the distribution of times for which ϕ starts to grow.

As in §3.1, we will assume sufficiently fast initial decay that we may take initial conditions to be $\phi(0) = 0$. The solution to (4.3) is then given by

$$\phi(s) = \xi \int_0^s \frac{1}{\varepsilon}\beta(\tau) \exp\left(-\frac{1}{\varepsilon}\int_s^\tau \alpha(\rho)d\rho\right) d\tau. \tag{4.4}$$

As in §3.1, we apply Laplace's method to further simplify this as follows. Let s_p be such that

$$\alpha(s_p) = 0. \tag{4.5}$$

Then from Laplace's Method (3.6), (4.4) yields

$$\phi(s) \sim \sqrt{\frac{2\pi}{\alpha'(s_p)\varepsilon}}\beta(s_p)\xi \exp\left(\frac{1}{\varepsilon}\int_{s_p}^s \alpha(\rho)d\rho\right). \tag{4.6}$$

The blow-up time s_b satisfies $|\phi(s_b)| = r$. To determine the distribution of the blow-up time, we define the cumulitive distribution function $F(s)$ to be

$$F(s) := P(|\phi(s)| \leq r).$$

Then

$$\begin{aligned} F(s) &= P\left(|\xi| \leq \frac{\exp\left(-\frac{1}{\varepsilon}A(s)\right)}{\eta}\right) \\ &= \frac{2}{\sqrt{2\pi}}\int_0^{\frac{\exp\left(-\frac{1}{\varepsilon}A(s)\right)}{\eta}} e^{-z^2/2}dz, \end{aligned} \tag{4.7}$$

where we defined

$$\eta = \frac{1}{r}\sqrt{\frac{2\pi}{\alpha'(s_p)\varepsilon}}\beta(s_p) \ll 1; \text{ and } A(s) = \int_{s_p}^s \alpha(\rho)d\rho. \tag{4.8}$$

Because of the exponential growth in the upper limit of the integral, $F(s)$ exhibits sharp transition from zero to one around the point where $\frac{\exp\left(-\frac{1}{\varepsilon}A(s)\right)}{\eta} \sim 1$. In other words, let s_d be defined through

$$\frac{\exp\left(-\frac{1}{\varepsilon}A(s_d)\right)}{\eta} = 1.$$

or

$$\int_{s_p}^{s_d} \alpha(\rho)d\rho = -\varepsilon \ln\left(\frac{1}{r}\sqrt{\frac{2\pi}{\alpha'(s_p)\varepsilon}}\beta(s_p)\right). \tag{4.9}$$

Then we have the following dichotamy:

$$F(s) \sim \begin{cases} 0 & \text{if } (s-s_d)/\varepsilon \ll 1 \\ 1 & \text{if } (s-s_d)/\varepsilon \gg 1 \end{cases}$$

We can capture the shape of this transition by expanding s as

$$s = s_d + \varepsilon t.$$

Then Taylor expansion around s_d yields

$$\frac{\exp\left(-\frac{1}{\varepsilon}A(s)\right)}{\eta} \sim \exp\left(-\alpha(s_d)t\right)$$

and

$$F(s) \sim \frac{2}{\sqrt{2\pi}} \int_0^{\exp(-\alpha(s_d)t)} e^{-z^2/2}dz.$$

It follows that the density distribution of blow-up time is given by

$$F'(s) \sim \frac{2}{\sqrt{2\pi}} \frac{\alpha\left(s_d\right)}{\varepsilon} \exp\left(-\frac{\exp\left(-2\alpha(s_d)\frac{s-s_d}{\varepsilon}\right)}{2}\right) \exp\left(-\alpha(s_d)\frac{s-s_d}{\varepsilon}\right). \tag{4.10}$$

We summarize this in the following theorem:

Theorem 1 *Let $f(s)$ be the distribution of the blow-up time for the ODE (4.2), that is, the probability that $|\phi(s)| \geq r$. Then $f(s)$ is given by*

$$f(s) = \frac{\alpha(s_d)}{\varepsilon}\hat{f}\left(\alpha(s_d)\frac{s-s_d}{\varepsilon}\right), \tag{4.11}$$

where s_d is defined implicitly through

$$\int_{s_p}^{s_d} \alpha(\rho)d\rho = -\varepsilon \ln\left(\frac{1}{r}\sqrt{\frac{2\pi}{\alpha'(s_p)\varepsilon}}\beta(s_p)\right) \tag{4.12}$$

and $\hat{f}(z)$ is given by

$$\hat{f}(s) := \sqrt{\frac{2}{\pi}} \exp\left(-\frac{\exp\left(-2z\right)}{2}\right) \exp\left(-z\right). \tag{4.13}$$

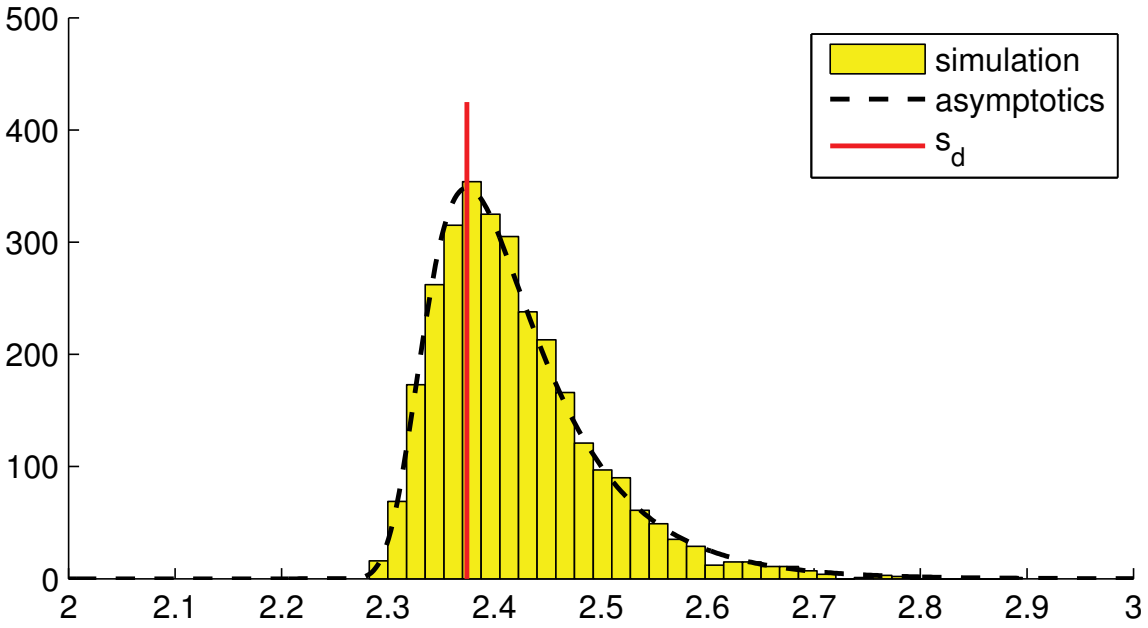

Figure 4.1: Comparison of the blow-up time for the ODE (4.2): full simulations versus asymptotic distribution (4.11). Here, $\alpha(s) = -1 + s$, $\beta(s) = 1$, $\sigma_0 = 10^{-5}$, $\varepsilon = 0.1$ and $r = 1$. Histogram shows the result of 3000 simulations using the exact solution to the ODE (4.2).

Note that the form (4.13) of the distribution is the same (up to shifts and translations) regardless of the choice of $\alpha(s), \beta(s)$. In this sense, (4.13) represents a *canonical* distribution for the blow-up times.

The mean $\mu = \int_{-\infty}^{\infty} f(s)sds$ is also easily computed as follows. Changing variables $z = \alpha(s_d)\frac{s-s_d}{\varepsilon}$ we obtain

$$\begin{aligned}\int_0^{\infty} f(s)sds &\sim \frac{2}{\sqrt{2\pi}}\int_{-\infty}^{\infty} \exp\left(-\frac{\exp(-2z)}{2}\right)\exp(-z)\left(\varepsilon\frac{z}{\alpha(s_d)} + s_d\right)dz \\ &= s_d + \frac{\varepsilon}{\alpha(s_d)}\frac{2}{\sqrt{2\pi}}\int_{-\infty}^{\infty} \exp\left(-\frac{\exp(-2z)}{2}\right)\exp(-z)\,z dz.\end{aligned}$$

The integral above can be evaluated with the help of Maple as follows:

$$\begin{aligned}&\frac{2}{\sqrt{2\pi}}\int_{-\infty}^{\infty} \exp\left(-\frac{\exp(-2z)}{2}\right)\exp(-z)\,z dz \\ &= \frac{1}{\sqrt{2\pi}}\int_0^{\infty} \exp\left(-\frac{u^2}{2}\right)\ln\left(\frac{1}{u}\right)du \\ &= (\ln 2 + \gamma)/2 = 0.635181.\end{aligned}$$

Here, $\gamma = 0.577$ is the Euler's constant. Similarly, we compute the variance:

$$\begin{aligned}
var &= \int f(s)\,(s-\mu)^2\,ds \\
&= \frac{2}{\sqrt{2\pi}}\int_{-\infty}^{\infty}\exp\left(-\frac{\exp(-2z)}{2}\right)\exp(-z)\left(\varepsilon\frac{z}{\alpha(s_d)}+s_d-\mu\right)^2 dz \\
&= \frac{2}{\sqrt{2\pi}}\left(\frac{\varepsilon}{\alpha(s_d)}\right)^2\int_{-\infty}^{\infty}\exp\left(-\frac{\exp(-2z)}{2}\right)\exp(-z)\,(z-(\ln 2+\gamma)/2)^2\,dz \\
&= \frac{2}{\sqrt{2\pi}}\left(\frac{\varepsilon}{\alpha(s_d)}\right)^2\int_{0}^{\infty}\exp\left(-\frac{u^2}{2}\right)u\,(-\ln u-(\ln 2+\gamma)/2)^2\,du \\
&= \left(\frac{\varepsilon}{\alpha(s_d)}\right)^2\frac{\sqrt{2\pi}}{24}\left(24(\ln 2)^2+\pi^2\right) \\
&= 2.2351\left(\frac{\varepsilon}{\alpha(s_d)}\right)^2,
\end{aligned}$$

where we used Maple to symbolically evaluate the integral. We summarize our calculations as follows:

Theorem 2 *The distribution (4.11) has a mean and standard deviation given by*

$$mean = s_d + \varepsilon\frac{(\ln 2+\gamma)/2}{\alpha(s_d)};$$
$$std = \frac{\varepsilon}{\alpha(s_d)}\left(\frac{\sqrt{2\pi}}{24}\left(24(\ln 2)^2+\pi^2\right)\right)^{1/2}.$$

This result shows that, to leading order, the mean is given by s_d. In fact, s_d is precisely the maximizer of the distribution $f(s)$. The "true" mean is close to it. In addition, the computation of the standard deviation shows that the distribution concentrates around s_d.

We now validate Theorem 2 using numerics. Choose

$$\alpha(s) = -1+s; \quad \beta(s) = \sigma_0.$$

Then $s_p = 1$ and (4.9) becomes

$$(s_d-1)^2 = -2\varepsilon\ln\left(\frac{1}{r}\sqrt{\frac{2\pi}{\varepsilon}}\sigma_0\right). \tag{4.14}$$

whereas the solution to (4.2) where $\alpha(s) = -1+s$ and $\beta(s) = \sigma_0$ has the exact form:

$$\phi(s) = \sigma_0\xi\sqrt{\frac{\pi}{2\varepsilon}}\exp\left(\frac{(-1+s)^2}{2\varepsilon}\right)\left\{\mathrm{erf}\left(\sqrt{\frac{1}{2\varepsilon}}\right)+\mathrm{erf}\left(\sqrt{\frac{1}{2\varepsilon}}(s-1)\right)\right\}.$$

We take $\varepsilon = 0.1,\ \sigma_0 = 10^{-5}$, and $r = 1$. We then solve the ODE 3000 times. The corresponding distribution of the blowup times $|\phi(s)| = r$ is shown as a histogram in Figure 4.1. It compares very well with the asymptotic prediction (dashed line) given by Theorem 1.

4.2 Single PDE

We now consider the following PDE with Dirichlet boundary condition in the domain $(0, \pi)$,

$$u_t = u_{xx} + a(\varepsilon t)u - u^3 + \sigma_0 \sum_{m=0}^{\infty} \xi_m \sin(mx), \tag{4.15}$$

where $a = \varepsilon t$. Linearizing analysis around the zero steady state $u(x,t) = 0 + \sum_m \phi_m(t) \sin(mx)$, we obtain

$$\varepsilon \frac{d}{ds}\phi_m = (-m^2 + s)\phi_m + \sigma_0 \xi_m, \quad m = 1, 2, \ldots \tag{4.16}$$

This is precisely of the form of the ODE (4.2) with

$$\alpha(s) = -m^2 + s; \quad \beta(s) = \sigma_0. \tag{4.17}$$

As in §3.1, given a positive constant r, we define the blow-up distribution corresponding to each mode m to be the first time s such that $|\phi_m(s)| = r$. These distributions are determined in Theorem 1 for each individual mode $m = 1, 2, \ldots$. Similarly, we define the blow-up distribution for the solution u to be the first time such that $|u| = r$.

Figure 4.2 shows the blowup distributions for ϕ_m with $\sigma_0 = 0.03, \varepsilon = 0.1$ and $r = 0.05$, as given by Theorem 1. As can be seen from this figure, these distributions do not overlap, and the mode $m = 1$ blows up before any other. Therefore the overall blowup distribution for u should coincide exactly with that of ϕ_m, $m = 1$.

Figure 4.3 and Figure 4.4 show the full numerical simulations of the single PDE (4.15), where we plot $\max_x |u|$ as a function of $s = \varepsilon t$. We used implicit-explicit finite differences method similar to that used in §3.1 to numerically compute the solution. The initial condition is $u = 0$. For each parameter set, several simulations are shown starting with different random seeds. The blow-up times appear to cluster closely

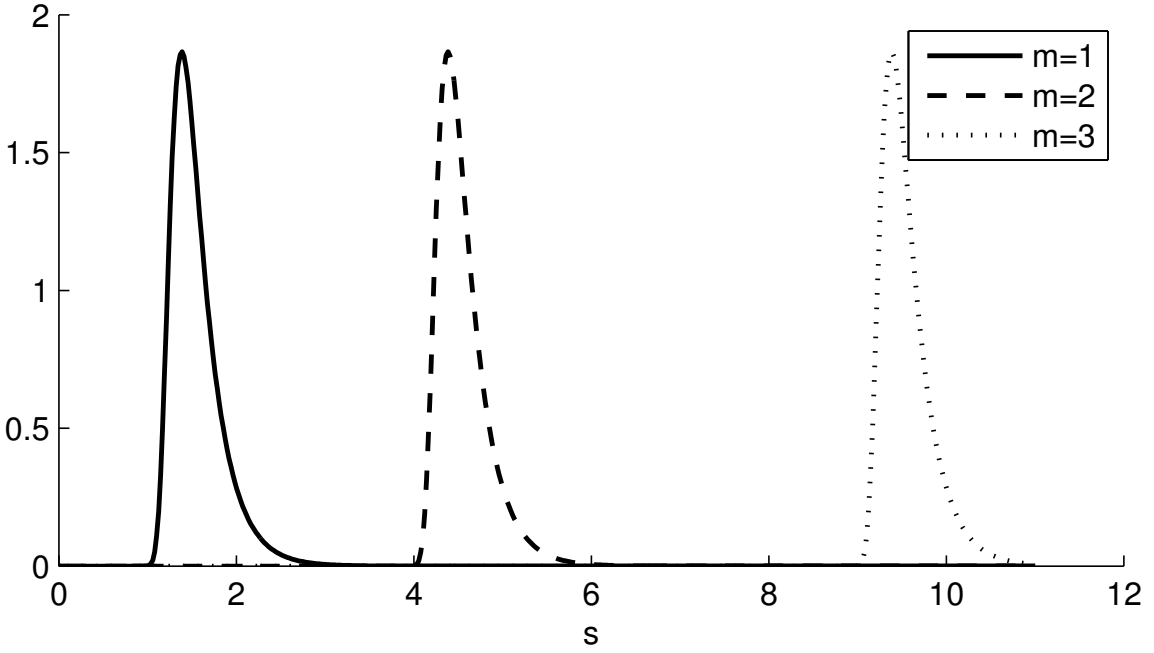

Figure 4.2: Asymptotic blowup distributions of modes ϕ_m from (4.9) with $r = 0.05$, $\sigma_0 = 0.03$, $\varepsilon = 0.1$, as given by Theorem 1. Note that the distributions do not overlap.

together. This is indeed predicted by Theorem 2, which shows that the standard deviation of the blow-up distribution is of $O(\varepsilon)$.

We also compare the density distribution of the blow up time s with the histogram obtained by full simulation. To obtain the full numerical results of blow-up time, we run the simulation for 2000 times by using the software Matlab, as shown in Figure 4.5 and Figure 4.6, and excellent agreement can be observed between the density function and the numerical results.

4.3 Klausmeier model

We now consider the simple case of Klausmeier model studied in (3.14) but with purely spatial noise

$$\begin{cases} \frac{\partial n}{\partial t} = \delta \frac{\partial^2 n}{\partial x^2} + n^2 w - n, \\ 0 = \frac{\partial^2 w}{\partial x^2} + a(\varepsilon t) - w - n^2 w + \sigma_0 \sum_{m=0}^{\infty} \xi_m \cos(mx). \end{cases} \tag{4.18}$$

Using the linearization

$$n = n_+ + \sum \phi_m(t) \cos(mx), \quad w = w_+ + \sum \psi_m(t) \cos(mx),$$

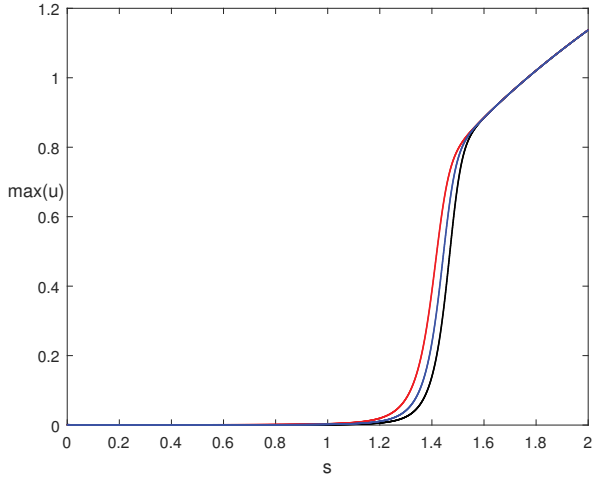

Figure 4.3: Evolution of the singular PDE with purely spatial noise and slow drift with $\varepsilon = 0.02$, $\sigma_0 = 0.0005$. The simulation is ran three times on a domain $L = \pi$ with Dirichlet boundary condition.

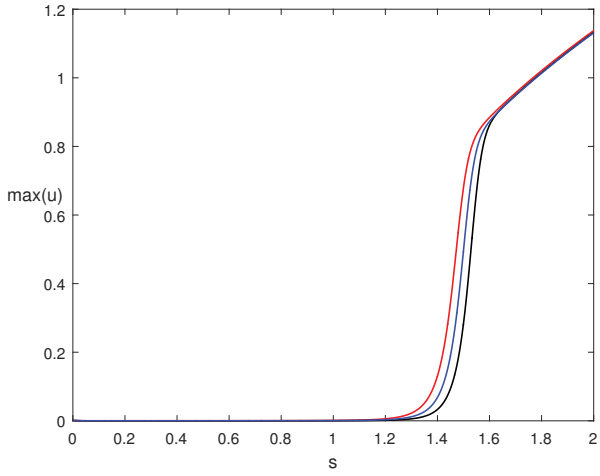

Figure 4.4: Evolution of the singular PDE with purely spatial noise and slow drift with $\varepsilon = 0.02$, $\sigma_0 = 0.0001$. The simulation is ran three times on a domain $L = \pi$ with Dirichlet boundary condition.

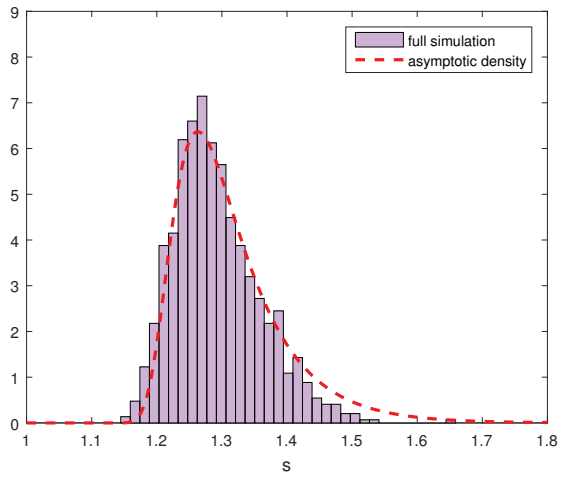

Figure 4.5: Numerical verification of density distribution of blow-up time with $\varepsilon = 0.02, \sigma_0 = 0.0005$ and $r = 0.05$.

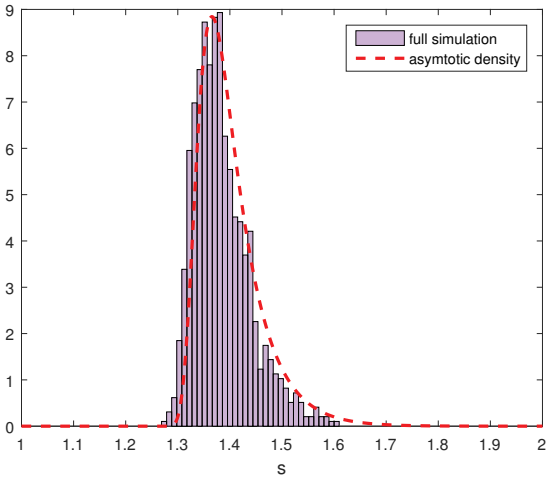

Figure 4.6: Numerical verification of density distribution of blow-up time with $\varepsilon = 0.02, \sigma_0 = 0.0001$ and $r = 0.05$.

we then obtain, along each mode,

$$\varepsilon\phi_s = \alpha(s)\phi + \beta(s)\xi_m, \tag{4.19}$$

where $\alpha(s)$ and $\beta(s)$ are same as in (3.20) and ξ_m is independent of time. Similarly to the cubic model (4.15), Theorem 1 then yields the distribution of blow-up time for each of the mode separately. However when the domain is large, these modes *overlap*. Consider, for example, the domain size $L = 20$ with $\varepsilon = 0.001, r = 0.05$, and $\sigma_0 = 0.0001$. The six most unstable modes are shown in Figure 4.7. Note that they have significant overlap. As a result, no single mode can predict the overall blowup distribution obtained by the full simulation (here the blow up time is defined such that $\max(n) - \min(n)$ first exceeds $2r = 0.1$) – also shown in Figure 4.7.

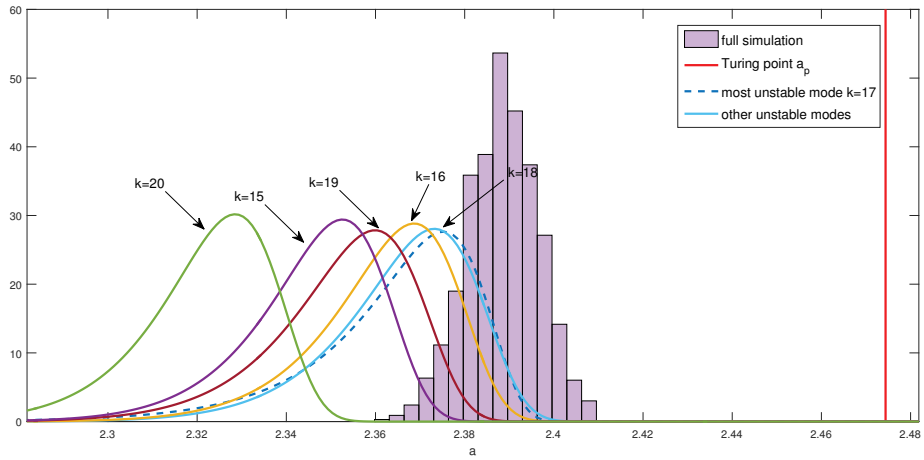

Figure 4.7: Asymptotic blowup distributions of modes ϕ_m from (4.19) for the Klausmeier model, compared with the blowup distribution for of the full system. Parameter values are $r = 0.05, \varepsilon = 0.001, \sigma_0 = 0.00001$ and $\delta = 0.05$, $a(\varepsilon t)$ is taken as $3 - \varepsilon t$. Note that the distributions for individual modes overlap, so that no single mode can predict the overall blowup distribution.

4.4 Conclusions

In this chapter we have considered PDE's driven by purely spatial (not spatio-temporal) noise. By decomposing the dynamics along fourier modes, we have obtained linear deterministic ODE's but with random forcing (4.2). In the case where

domain size is sufficiently small, the blowup profile along each mode is well separated from all others. As a result, the blowup distribution of the most unstable mode yields the overall blowup distribution of the full system. However in the case of large domain, the blowup distributions along individual modes overlap. In this case, no individual mode is a good predictor of an overal blowup profile. Understanding how the various modes interact is the subject of future research.

Chapter 5

Conclusion

In this thesis we studied the combined effect of noise and slow parameter drift on the onset of Turing bifurcation by looking for the blow up time at which the solution starts to deviate quickly from the homogeneous steady state. We considered two models: a single PDE, and a modified version of Klausmeier model which is a system of two PDE's. We applied and extended the methods used in [1] to more general class of systems, as well as to the case of purely spatial (not spatio-temporal) noise.

In §3.2 we reviewed the results of [1] as applied to the simplest case of Klausmeier model (1.3) corresponding to $b = 0, c = 0$. We then extended the method to cover the case of a system ($b \neq 0$), and complex eigenvalues ($c \neq 0$). When $b \neq 0$, linearization results in two coupled ODE's (rather than a single equation when $b = 0$). We approximated the resulting system by a single equation, using adjoint eigenvectors/eigenvalue pairs. At the end, we obtained a single Ornstein-Uhlenbeck process and then the analysis proceeded the same as in §3.2. Moreover, we compared the blow up point between analysis and numerics with respect to b. When $c \neq 0$, $\alpha(s)$ and $\beta(s)$ in (3.20) are not real but complex. In this case, we chose the real part of new $\alpha(s)$ and $\beta(s)$ and find out the "take-off" value using the similar analysis. In all cases, we performed numerical simulations and good agreement were observed between analysis results and full simulations.

To study the combined effect of noise and slow parameter drift, we considered two alternative definitions of the "blowup time". The first definition – and the one used in [1] – is to look at the variance of the density distribution of the solution, and to define the blowup to occur when this variance first exceeds one. This gives a single number for the blowup time, which can be approximated by decomposing the solution along its Fourier modes near the homogeneous steady state. A more detailed definition is to consider the blowup time to be a distribution itself, rather than just a single number. The latter definition provides for a more refined picture of the solution

blowup. Both of these two notions involve the combined effect of noise and the slow passage parameter.

We obtained two cases when looking for the distribution of blowup time. In the case where the density distributions for various modes do not overlap too much, the overall density distribution of blow up time is exactly the same as the mode that blows up first. This is the case in particular for the single PDE system (3.1 and 4.15) and more generally, when the domain size is sufficiently small. However when the domain size is sufficiently large, such as an example of Klausmeier considered in §4.3, density distributions for various modes overlap with each other and then the solution may blow up earlier than any of the individual modes. It is an open problem to understand this interaction which will enable us to describe the overall distribution of delay in Turing bifurcation.

In §4 we studied the profile of the blowup distributions for the case of a purely spatial noise. In this case, we obtained a linear deterministic ODE's but with random variables (4.2) rather than a Ornstein-Uhlenbeck process. A canonical density distribution of the blow up time such that $|\phi| = r$ is obtained (see Theorem 1). We also applied this method to the same problems in §3 and the density functions of blow up time for each mode are in the same form as in Theorem 1 but with different scaling.

There are several outstanding questions that we plan to address in the future. First, we would like to study the distribution of the blowup points when the domain is large. As can be seen in Figure 4.7, in this case the individual modes are not good predictors of the overall distribution and rather, the study of combined distribution is needed. Another interesting question is to study the effect of oscillations on bifurcation delays. This is the case, for example, with the Klausmeier model when b is sufficiently large. More general systems cases can also be considered for future work. We would also like to extend these results to higher dimensions.

Bibliography

[1] Yuxin Chen, Theodore Kolokolnikov, Justin Tzou, and Chunyi Gai. Patterned vegetation, tipping points, and the rate of climate change. *European Journal of Applied Mathematics*, pages 1–14, 2015.

[2] AK Kapila. Arrhenius systems: dynamics of jump due to slow passage through criticality. *SIAM Journal on Applied Mathematics*, 41(1):29–42, 1981.

[3] TT Tsotsis, RC Sane, and TH Lindstrom. Bifurcation behavior of a catalytic reaction due to a slowly varying parameter. *AIChE journal*, 34(3):383–388, 1988.

[4] Albert Goldbeter and Lee A Segel. Control of developmental transitions in the cyclic amp signalling system of dictyostelium discoideum. *Differentiation*, 17(1-3):127–135, 1980.

[5] Robert M May. Thresholds and breakpoints in ecosystems with a multiplicity of stable states. *Nature*, 269(5628):471–477, 1977.

[6] Marten Scheffer, Steve Carpenter, Jonathan A Foley, Carl Folke, and Brian Walker. Catastrophic shifts in ecosystems. *Nature*, 413(6856):591–596, 2001.

[7] Millennium Ecosystem Assessment et al. *Ecosystems and human well-being*, volume 5. Island Press Washington, DC, 2005.

[8] Steven M Baer, Thomas Erneux, and John Rinzel. The slow passage through a hopf bifurcation: delay, memory effects, and resonance. *SIAM Journal on Applied mathematics*, 49(1):55–71, 1989.

[9] Paul Mandel and Thomas Erneux. The slow passage through a steady bifurcation: delay and memory effects. *Journal of statistical physics*, 48(5-6):1059–1070, 1987.

[10] Christian Kuehn. A mathematical framework for critical transitions: Bifurcations, fast–slow systems and stochastic dynamics. *Physica D: Nonlinear Phenomena*, 240(12):1020–1035, 2011.

[11] Justin C Tzou, Michael J Ward, and Theodore Kolokolnikov. Slowly varying control parameters, delayed bifurcations, and the stability of spikes in reaction–diffusion systems. *Physica D: Nonlinear Phenomena*, 290:24–43, 2015.

[12] Hassina Zeghlache, Paul Mandel, and C Van den Broeck. Influence of noise on delayed bifurcations. *Physical Review A*, 40(1):286, 1989.

[13] Paul Mandel. *Theoretical problems in cavity nonlinear optics*, volume 21. Cambridge University Press, 2005.

[14] Maxi San Miguel and Raul Toral. Stochastic effects in physical systems. In *Instabilities and nonequilibrium structures VI*, pages 35–127. Springer, 2000.

[15] R Kuske. Probability densities for noisy delay bifurcations. *Journal of statistical physics*, 96(3-4):797–816, 1999.

[16] S Varela, C Masoller, and AC Sicardi. Numerical simulations of the effect of noise on a delayed pitchfork bifurcation. *Physica A: Statistical Mechanics and its Applications*, 283(1):228–232, 2000.

[17] Paolo D'Odorico, Francesco Laio, and Luca Ridolfi. Noise-induced stability in dryland plant ecosystems. *Proceedings of the National Academy of Sciences of the United States of America*, 102(31):10819–10822, 2005.

[18] Paolo D'Odorico and Abinash Bhattachan. Hydrologic variability in dryland regions: impacts on ecosystem dynamics and food security. *Philosophical Transactions of the Royal Society B: Biological Sciences*, 367(1606):3145–3157, 2012.

[19] J Michael T Thompson and Jan Sieber. Climate tipping as a noisy bifurcation: a predictive technique. *IMA Journal of Applied Mathematics*, 76(1):27–46, 2011.

[20] G Broggi, Arrigo Colombo, Luigi A Lugiato, and Paul Mandel. Influence of white noise on delayed bifurcations. *Physical Review A*, 33(5):3635, 1986.

[21] MC Torrent and M San Miguel. Stochastic-dynamics characterization of delayed laser threshold instability with swept control parameter. *Physical Review A*, 38(1):245, 1988.

[22] Desmond J Higham. An algorithmic introduction to numerical simulation of stochastic differential equations. *SIAM review*, 43(3):525–546, 2001.

[23] Steven H Strogatz. *Nonlinear dynamics and chaos: with applications to physics, biology, chemistry, and engineering*. Westview press, 2014.

[24] Nils Berglund and Barbara Gentz. Pathwise description of dynamic pitchfork bifurcations with additive noise. *Probability theory and related fields*, 122(3):341–388, 2002.

[25] Christopher A Klausmeier. Regular and irregular patterns in semiarid vegetation. *Science*, 284(5421):1826–1828, 1999.

[26] Reinier HilleRisLambers, Max Rietkerk, Frank van den Bosch, Herbert HT Prins, and Hans de Kroon. Vegetation pattern formation in semi-arid grazing systems. *Ecology*, 82(1):50–61, 2001.

[27] Max Rietkerk, Pieter Ketner, Joep Burger, Bart Hoorens, and Han Olff. Multiscale soil and vegetation patchiness along a gradient of herbivore impact in a semi-arid grazing system in west africa. *Plant Ecology*, 148(2):207–224, 2000.

[28] Nadia Ursino and Samuel Contarini. Stability of banded vegetation patterns under seasonal rainfall and limited soil moisture storage capacity. *Advances in Water Resources*, 29(10):1556–1564, 2006.

[29] Vishwesha Guttal and C Jayaprakash. Self-organization and productivity in semi-arid ecosystems: Implications of seasonality in rainfall. *Journal of theoretical biology*, 248(3):490–500, 2007.

[30] Jonathan A Sherratt. Pattern solutions of the klausmeier model for banded vegetation in semi-arid environments ii: patterns with the largest possible propagation speeds. In *Proceedings of the Royal Society of London A: Mathematical, Physical and Engineering Sciences*, volume 467, pages 3272–3294. The Royal Society, 2011.

[31] Alan Mathison Turing. The chemical basis of morphogenesis. *Philosophical Transactions of the Royal Society of London B: Biological Sciences*, 237(641):37–72, 1952.

[32] AD Fokker. Die mittlere energie rotierender elektrischer dipole im strahlungsfeld. *Annalen der Physik*, 348(5):810–820, 1914.

[33] William Everett Ver Planck. Piston for internal-combustion engines., November 6 1917. US Patent 1,245,641.

[34] Andrei Kolmogoroff. Über die analytischen methoden in der wahrscheinlichkeitsrechnung. *Mathematische Annalen*, 104(1):415–458, 1931.

[35] Crispin Gardiner and Peter Zoller. *Quantum noise: a handbook of Markovian and non-Markovian quantum stochastic methods with applications to quantum optics*, volume 56. Springer Science & Business Media, 2004.

[36] Hannes Risken. Fokker-planck equation. In *The Fokker-Planck Equation*, pages 63–95. Springer, 1996.

[37] Zeev Schuss. *Stochastic Differential Equations*. Wiley Online Library, 1980.

[38] Mark H Holmes. *Introduction to perturbation methods*, volume 20. Springer Science & Business Media, 2012.

Appendices

CAMBRIDGE UNIVERSITY PRESS LICENSE TERMS AND CONDITIONS

Dec 21, 2015

This is an Agreement between Chunyi Gai ("You") and Cambridge University Press ("Cambridge University Press"). It consists of your order details, the terms and conditions provided by Cambridge University Press, and the payment terms and conditions.

All payments must be made in full to CCC. For payment instructions, please see information listed at the bottom of this form.

License Number	3773850253141
License date	Dec 21, 2015
Licensed Content Publisher	Cambridge University Press
Licensed Content Publication	European Journal of Applied Mathematics
Licensed Content Title	Patterned vegetation, tipping points, and the rate of climate change
Licensed Content Author	YUXIN CHEN, THEODORE KOLOKOLNIKOV, JUSTIN TZOU and CHUNYI GAI
Licensed Content Date	Jan 1, 0023
Volume number	26
Issue number	06
Start page	945
End page	958
Type of Use	Dissertation/Thesis
Requestor type	Author
Portion	Full article
Author of this Cambridge University Press article	Yes
Author / editor of the new work	Yes
Order reference number	None
Territory for reuse	World
Title of your thesis / dissertation	Delayed bifurcation onset of Turing instability and the effect of noise
Expected completion date	Dec 2015
Estimated size(pages)	52
Billing Type	Invoice
Billing Address	Chunyi Gai 4601 West 11th Ave., Vancouver None None Vancouver, BC V6R 2M6 Canada Attn: Chunyi Gai
VAT / Sales Tax	0.00 USD
Total	**0.00 USD**
Terms and Conditions	

TERMS & CONDITIONS

Cambridge University Press grants the Licensee permission on a non-exclusive non-transferable basis to reproduce, make available or otherwise use the Licensed content 'Content' in the named territory 'Territory' for the purpose listed

'the Use' on Page 1 of this Agreement subject to the following terms and conditions.

1. The License is limited to the permission granted and the Content detailed herein and does not extend to any other permission or content.
2. Cambridge gives no warranty or indemnity in respect of any third-party copyright material included in the Content, for which the Licensee should seek separate permission clearance.
3. The integrity of the Content must be ensured.
4. The License does extend to any edition published specifically for the use of handicapped or reading-impaired individuals.
5. The Licensee shall provide a prominent acknowledgement in the following format:
   author/s, title of article, name of journal, volume number, issue number, page references, , reproduced with permission.

Other terms and conditions:
v1.0